FINAL TECHNICAL REPORT
PROJECT A–3411

DESIGN, FABRICATION, AND TEST OF THE S–BAND TASA-II TELEMETRY ANTENNA SYSTEM

By
W. P. Cooke, J. E. Thompson, D. R. Blount,
B. M. Jenkins, and D. O. Gallentine

Prepared for
Kentron International, Inc.
Huntsville, Alabama 35802

Under
Purchase Order No. K151619-X
(Under Govt. Prime DASG60–82–C–0002)

Prepared by
Electromagnetic Effectiveness Division
Electronics and Computer Systems Laboratory

May 1984

GEORGIA INSTITUTE OF TECHNOLOGY
A Unit of the University System of Georgia
Engineering Experiment Station
Atlanta, Georgia 30332

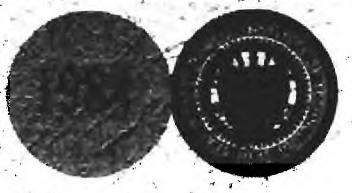

FINAL TECHNICAL REPORT

PROJECT A-3411

DESIGN, FABRICATION, AND TEST OF THE S-BAND TASA-II TELEMETRY ANTENNA SYSTEM

By

W. P. Cooke, J. E. Thompson, D. R. Blount,
B. M. Jenkins, and D. O. Gallentine

May 1984

Prepared for

Kentron International, Inc.
2003 Byrd Spring Road
Huntsville, Alabama 35802

Prepared by

Electromagnetic Effectiveness Division
Electronics and Computer Systems Laboratory
Engineering Experiment Station
Georgia Institute of Technology
Atlanta, Georgia 30332

FOREWORD

The development of the S-band TASA-II telemetry antenna system described in this final engineering report was accomplished by personnel of the Engineering Experiment Station at the Georgia Institute of Technology, Atlanta, Georgia 30332. The program was supported by Kentron International, Inc., 2003 Byrd Spring Road, Huntsville, Alabama 35802, under Purchase Order No. K151619-X (under Government Prime DASG60-82-C-0002). This project was designated by Georgia Tech as Project A-3411. Technical direction from the sponsor was provided by Mr. James B. Coon. This report covers work performed from 10 November 1982 through 1 June 1984, and the antenna system was shipped to Kwajalein on 25 August 1983.

The authors would like to acknowledge the support and helpful discussions provided by: (1) members of the Electromagnetic Effectiveness Division, including Dr. J. P. Montgomery and Dr. J. A. Fuller, and (2) members of Kentron International, including Messrs. P. H. Densford and J. B. Coon. The authors also acknowledge Messrs. R. E. Baugh and R. M. Ueberschaer for their contribution to this program. In addition, appreciation is expressed by the authors to Ms. Beatriz Gonzalez for her careful preparation of this manuscript.

Respectfully submitted,

William P. Cooke
Project Director

Approved:

Charles E. Ryan, Jr.
Chief,
EM Effectiveness Division

TABLE OF CONTENTS

LIST OF FIGURES

LIST OF FIGURES

LIST OF FIGURES

LIST OF TABLES

SECTION I
INTRODUCTION

A. Background

The personnel at the Electronics and Computer Systems Laboratory (ECSL), Engineering Experiment Station (EES), at Georgia Tech designed, fabricated, and tested an airborne S-band telemetry (TM) antenna system. This antenna development program was in support of efforts by Kentron International to develop a terminal area support aircraft (TASA) to collect TM data on inbound targets to the Kwajalein missile range. This antenna is referred to as the TASA-I TM antenna system, and further information about this antenna system is described in Reference 1.

The result from the TASA-I program was the development of a unique S-band TM antenna system that operates in the 2.2-2.3 GHz frequency range using a lightweight Luneberg lens. The antenna Luneberg lens aperture is illuminated by a four-element array consisting of four ortho-mode quad-ridge circular waveguide feeds. These devices are capable of instantaneous left -and right-hand-circular polarizations. The antenna system has four modes of operation; these modes are: (1) a manual mode where all four feeds can be individually selected, (2) an automatic mode where any feed can be automatically selected by the electronics depending upon which beam contains the largest signal, (3) a two-beam combine mode where two interior beams are coherently summed, and (4) a four-beam combine mode where all four feeds are coherently summed. In the automatic mode, the antenna is an electronic beam switch system that provides approximately the same pattern coverage as the four-beam sum mode with more antenna gain than the four-beam sum mode. Some of the more salient featues of the TASA-I antenna system include: (1) antenna system noise temperature of 239°K, (2) minimum RF system gain of 39 dB (4-beam combine mode), (3) minimum receiver sensitivity of -99 dBm (used for automatic beam selection), (4) 10 nanosecond (maximum) beam switching time, and (5) 156 lb. total weight for the antenna system.

B. Summary

This report summarizes the work accomplished by the ECSL personnel to design and fabricate a TASA-II antenna system. Pictures of the antenna

system are shown in Figure 1. The TASA-II antenna system contains important improvements over the TASA-I antenna system. The antenna system is divided into five subsystems, and these are: (1) mechanical structure, (3) radome assembly, (3) antenna feeds, (4) microwave circuitry, and (5) electronic circuitry. Depending on the requirement, changes were made to each of these subsystems, and these are described in detail in Section II. All of the modifications to the TASA-II antenna improved its performance; perhaps the most significant improvement was the reduction of the antenna axial ratio performance relative to the TASA-I antenna. During a previously sponsored Kentron program [2], two problem areas with the Luneberg lens antenna were identified; these problem areas were: (1) a feed-ground plane resonance phenomena, and (2) anisotropic behavior in the Luneberg lens. This program showed that by changing the antenna ground plane design and the orientation of the Luneberg lens, the mainbeam axial ratio could be improved. These results were incorporated into the TASA-II TM antenna system. The entire feed-ground plane structure was modified to defeat the resonance problem and simplify maintenance procedures. Measurements and tests shown in this report on the TASA-II antenna system demonstrate that all modifications have improved the antenna system; in particular, the mainbeam axial ratio for the TASA-II antenna is on the order of 2-3 dB.

The remainder of this report provides further detailed descriptions regarding the design and construction of the TASA-II antenna. Section II describes the improvements made to the TASA-II antenna system. Section III discusses the antenna system fabrication and presents test and measurement results. Conclusions and recommendations for future antenna work are presented in Section IV.

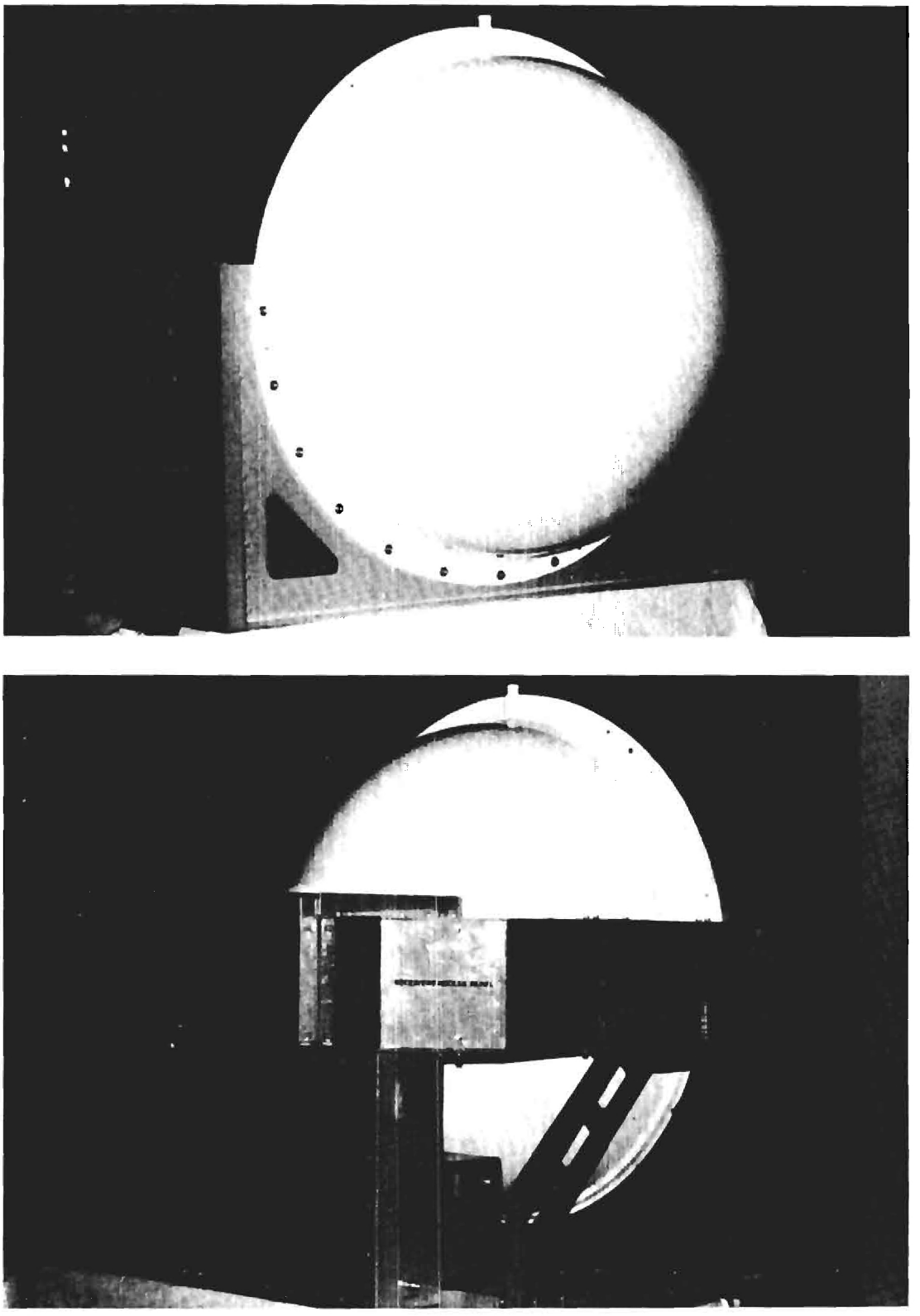

Figure 1. Photographs of the TASA-II antenna system.

SECTION II
TASA-II TM ANTENNA SYSTEM DESIGN

A. Introduction

The design of the TASA-II TM antenna system is the same as the design of the TASA-I except for a series of important modifications. The TASA TM antenna system is divided into five subsystems; these are the: (1) mechanical structure, (2) radome assembly, (3) antenna feeds, (4) microwave circuitry, and (5) electronic circuitry. Various modifications were made to each subsystem, and this section of the report describes all of the design modifications made to the TASA-II TM antenna system.

B. Mechanical Structure

The quad-ridge feed support and ground-plane structures were redesigned. The new design is a feed carriage assembly that is totally removable from the mechanical structure. The low-noise amplifiers (LNAs) and low-loss preselect filters are mounted on a carrier plate that can be easily removed from the feed carriage assembly. These devices slide out from the rear of the feed carriage assembly. A drawing of the TASA-II mechanical structure design is shown in Figure 2. Notice that the feed carriage assembly is larger than the surrounding structure to accommodate the additional components. Figure 3 shows two views of the feed carriage assembly. A ground plane is part of the feed carriage assembly, and it is mounted at the feed element apertures. The ground plane uses flat segments at the intersection of the feed element aperture. In addition, an electrical ground path is provided by a RFI/EMI mesh at the intersection of the feed element aperture and the ground plane (see Figure 3). Recall that prior work [2] showed that this ground path would defeat a resonance problem that degraded the antenna axial ratio performance on TASA-I.

C. Radome Assembly

The radome assembly was not modified except for its alignment relative to the mechanical structure. The work described in Reference 2 identified that the Luneberg lens exhibited anisotropic properties such as depolarization of an incident field. This characteristic was found to be orientation dependent. As a result, changing the Luneberg lens orientation

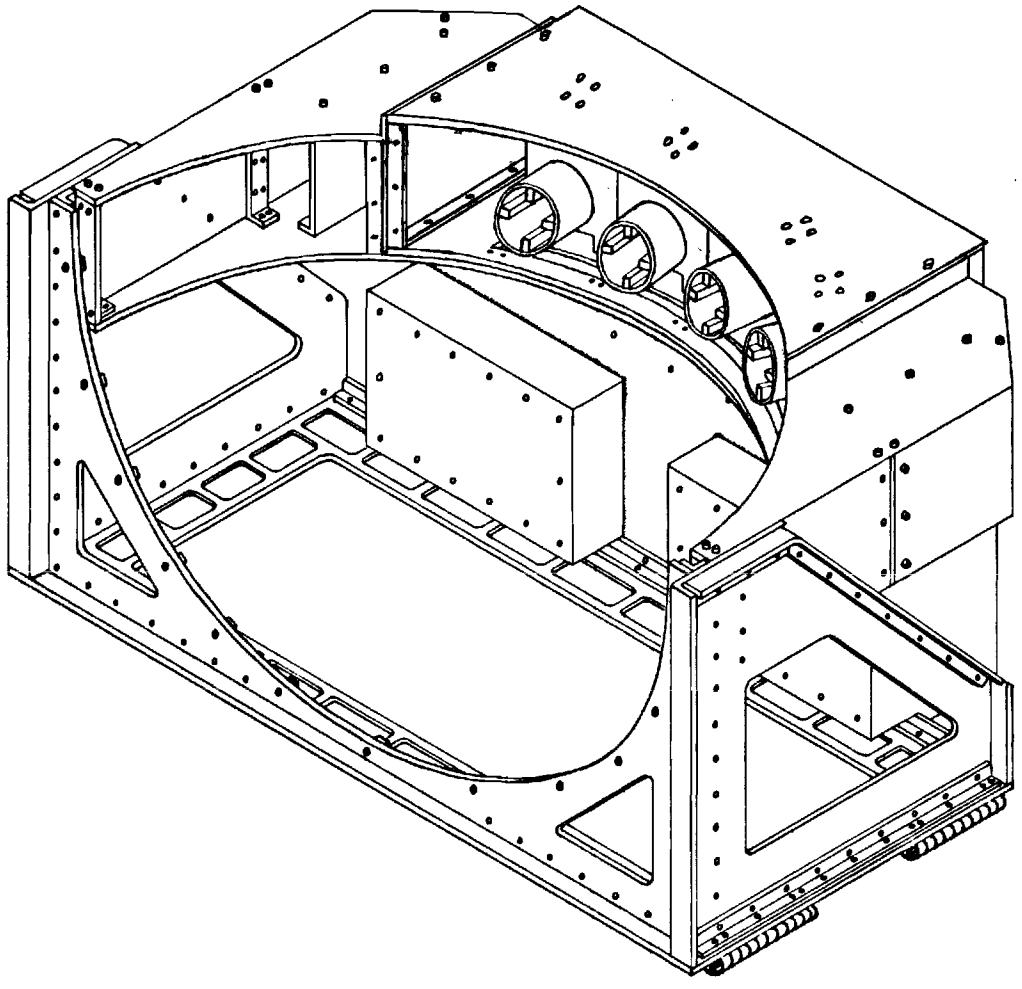

Figure 2. Drawing of the final design for the TASA-II mechanical assembly.

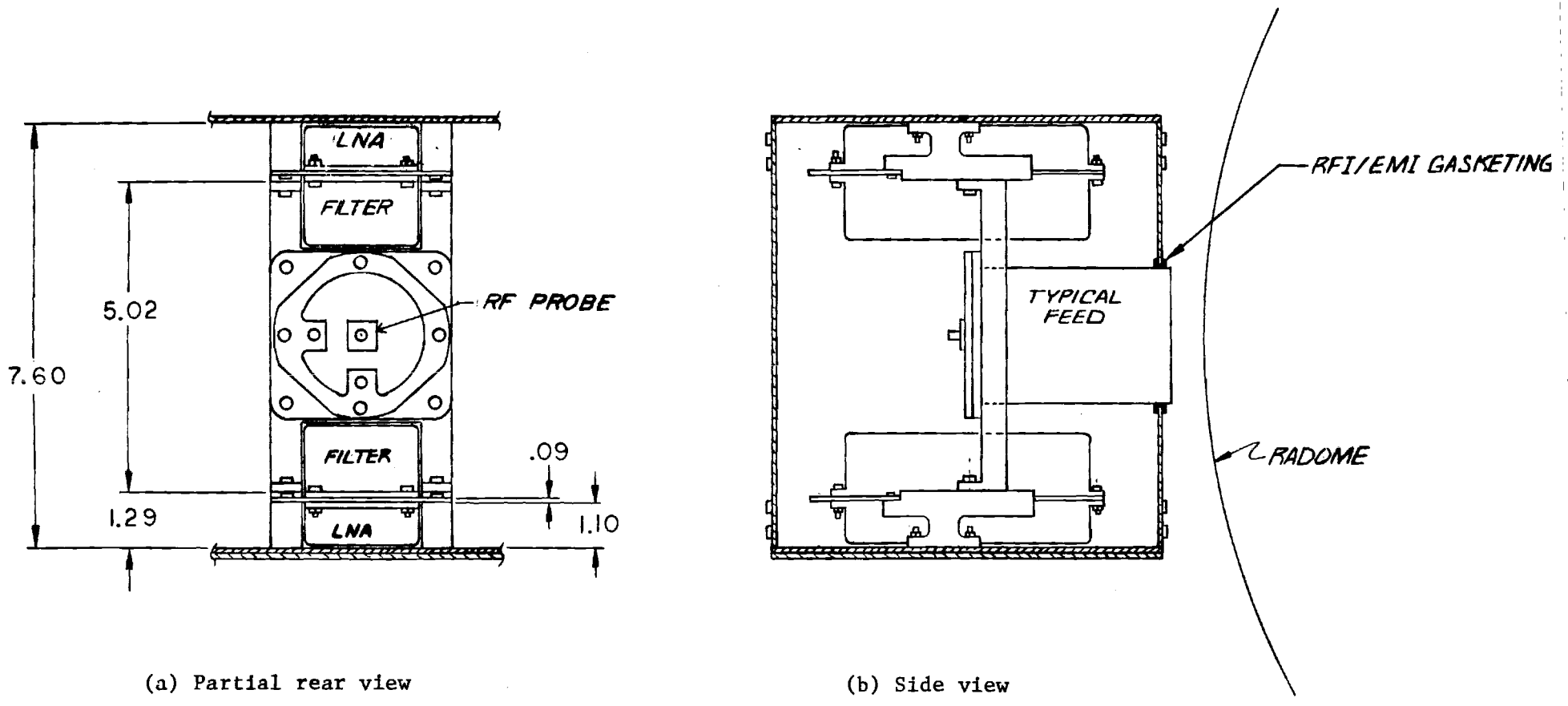

(a) Partial rear view

(b) Side view

Figure 3. Two views of the feed carriage assembly.

relative to the mechanical structure would improve the antenna system's axial ratio response.

D. Antenna RF Feeds

The antenna feed is composed of a electroformed quad-ridge element and a coax-to-waveguide transition mounted on an end plate. The electroform element remained unchanged; however, the feed element end plate was modified to accommodate a small RF probe. This device is an electrically small monopole mounted in the center of the base plate (see Figure 3). Each feed of the four element array has a RF probe driven by a four-way power divider. This design modification provides an easy method to inject a RF reference signal for calibration and test purposes. This technique was selected instead of signal injection using a stripline coupler. Signal injection using couplers would require a coupler in each of the eight signal paths and an eight-way power divider to drive each coupler input port. Relative to the RF probe approach, the coupler method suffers from increased insertion losses with the corresponding increases in system noise figure and increased microwave circuit complexity.

Tests were performed on a brassboard model of the feed with several monopole element lengths; the varying of the element length controls the amount of coupling between the probe input port and the feed output ports. Figures 4-5 present swept-frequency coupling results between the probe and feed output ports (including the 90° hybrid). The monopole element characteristics are shown in these figures. These results demonstrate the feasibility of this method and show a flat response with about -50 dB coupling. In addition, tests with the Luneberg lens showed that the degree of coupling was insensitive to structures around the antenna. Thus, because of the simplicity and effectiveness of the RF probe method, it was selected to inject RF signals into the antenna system.

E. Microwave Circuitry

As shown in Figure 6, significant modifications were made to the microwave circuitry. Notice that the 90° hybrids are now located at the feed element outputs, and preselect filters were added to the signal paths to protect the LNAs. These devices are evanescent TE mode filters with high-Q cavities that achieve large stopband and low passband attenuation.

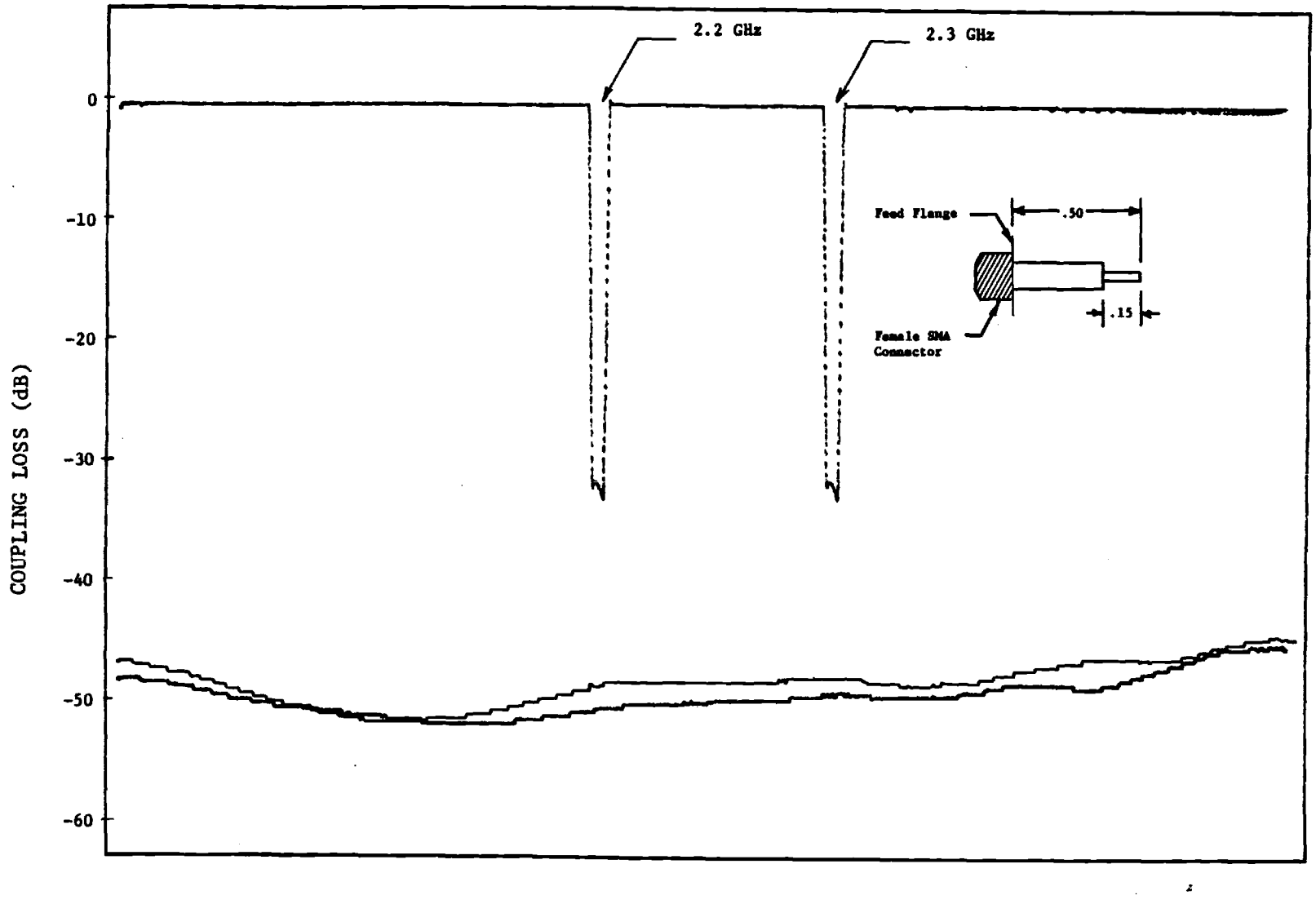

Figure 4. Swept-frequency coupling between the probe and feed mounted in the brassboard ground plane.

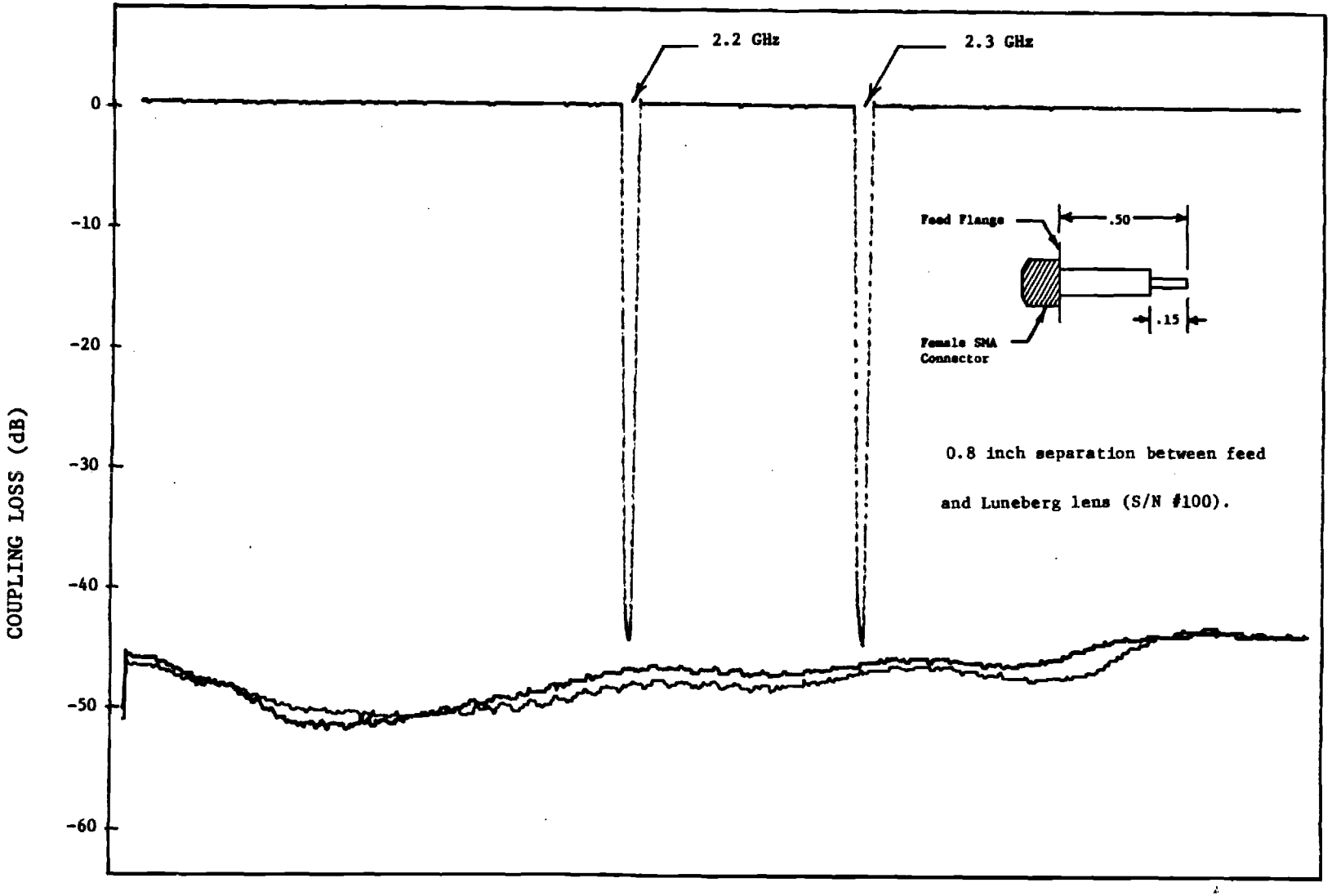

Figure 5. Swept-frequency coupling between the probe and feed mounted in brassboard ground plane with the Luneberg lens.

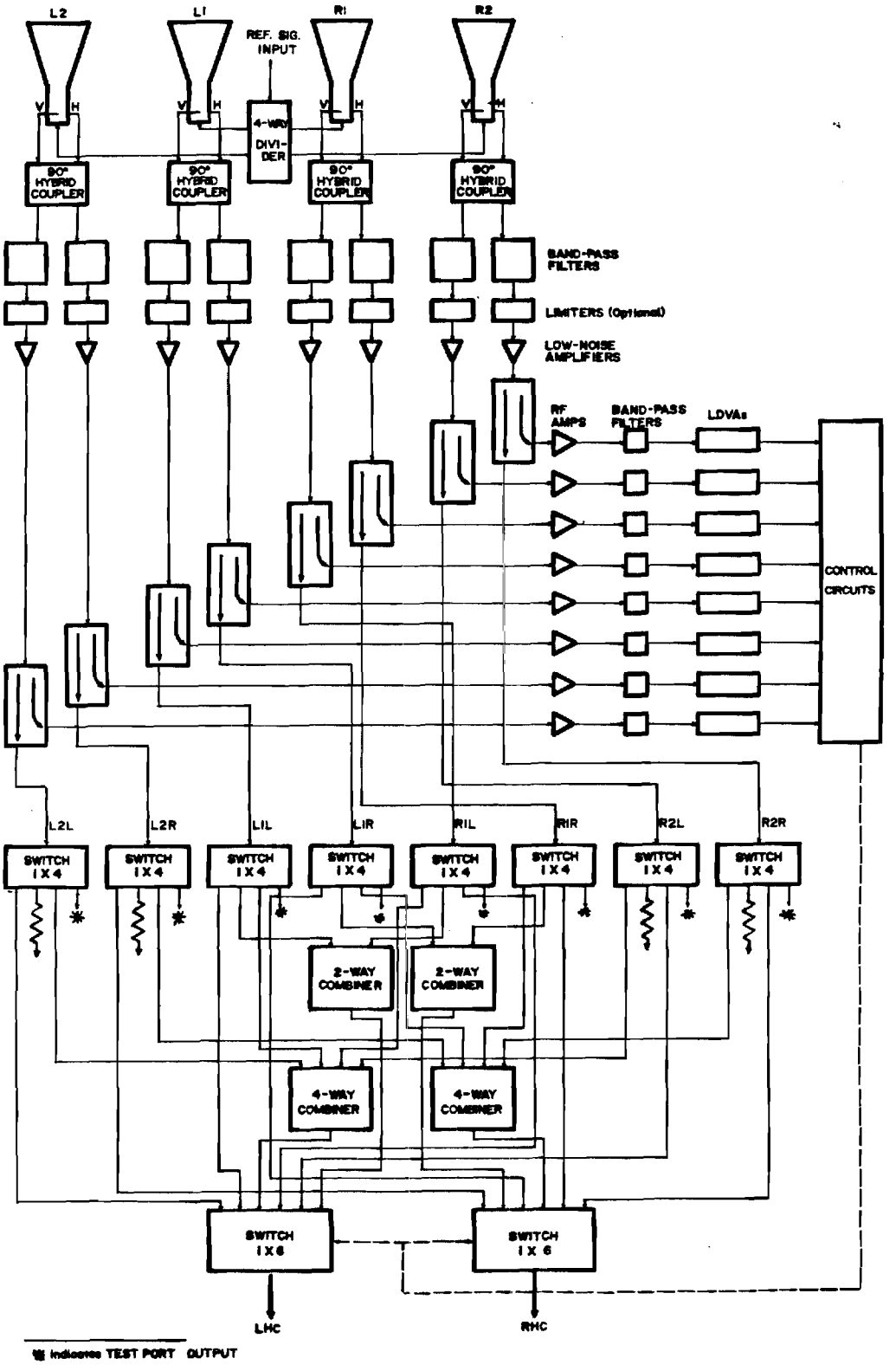

Figure 6. Schematic diagram of the antenna microwave circuitry.

The bandpass filter characteristics are shown in Table I. Notice that the filter has a maximum of 0.4 dB insertion loss across the 2.2-2.3 GHz range. Also, for proper performance, these devices must phase track.

Several LNA characteristics were changed including the RF gain and size. The LNA characteristics are presented in Table II; the gain was reduced to 40 dB. Although the specified LNA noise figure was 1.1 dB, the delivered units exhibited significantly less noise figure; the actual LNA noise performance will be discussed in the next section. Also, its size was reduced to facilitate mounting in the feed carriage assembly. In addition, a bayonet connector replaced solder terminals to supply DC voltage to the LNAs. The RF limiters are optional devices that can be used to protect the LNAs. These units were available on the TASA-I system and are "screw-on" devices that can be attached to the LNA input. They will protect the LNA from input signals as large as six watts with a maximum of 0.2 dB insertion loss. However, unless large inband RF signals are expected, the bandpass filters should provide adequate LNA protection without the need of the RF limiters. Assuming the RF limiters are unnecessary, about 0.2 dB reduction in noise figure can be realized.

Following the LNAs, the microwave circuitry is essentially the same as the circuitry used on the TASA-I system. The 1-pole, 4-throw electromechanical switches route signals according to the antenna mode of operation. Notice that a diagnostic output port located on the switches has been added; an appropriately labeled switch located near the electromechanical switches controls this feature, and when activated, all RF signals are available at the electromechanical output ports. The two-way and four-way combiners provide the two-beam and four-beam sum modes. The 1-pole, 6-throw PIN-diode switches are the final devices in the network and are controlled by the system electronics to select the appropriate signal port depending on the mode of operation.

Observe in Figure 6 the three character alphanumeric code, such as R1R. This symbol identifies the antenna feed channel and polarization. As an example, the first two characters in R1R corresponds to feed R1 (Right-1), and the remaining R identifies right-hand-circular polarization. Therefore, channel L2L means feed L2 (Left-2) and left-hand-circular polarization.

TABLE I

LOW-LOSS BANDPASS FILTER SPECIFICATIONS

Performance	
Center Frequency	2250 MHz
Inband (2200 MHz to 2300 MHz) Insertion Loss (max)	0.4 dB
Inband Rippe (max)	±0.1 dB
Insertion Loss at 1890 MHz and 2610 MHz (min)	50 dB
Impedance	50 ohms
Inband VSWR (max)	1.5:1
Input Power (min)	5 Watts CW
Phase Match between Units (max)	±5°
Environmental	
Temperature	0° to 65° C
Humidity	10% to 95% relative
Altitude	0 to 3,000 m
Vibration	1.6 g's maximum for 5 to 55 Hz (operational environment) 3 g's maximum for 55 to 500 Hz (operational environment)
Shock	5 g's maximum for 45 msec (operational environment) 15 g's maximum for 11 msec (non-operational environment)

TABLE II

LNA SPECIFICATIONS

Performance	
Frequency Response (min)	2200-2300 MHz
Noise Figure @ 23°C (max)	1.1 dB
Noise Figure LNA + Limiter @ 23°C (max)	1.3 dB
Gain	40 dB
Gain Flatness	±0.5 dB
Gain Match (between units) over specified frequency and temperature ranges	1.0 dB
Power Output 1 dB comp. (min)	+10 dBm
Third Order Intercept Point (min)	+20 dBm
Phase Linearity	±5°
Phase Match (between units)	±5°
Impedance	50 ohms
VSWR (max) In/Out	1.3:1/1.5:1
Power (max)	+15 VDC @ 100 ma
Input Power with Limiter (min)	5 watts CW
Environmental	
Temperature	0° to 65°C
Humidity	10% to 95% relative
Altitude	0 to 3,000 m
Vibration	1.6 g's maximum for 5 to 55 Hz (operational environment) 3 g's maximum for 55 to 500 Hz (operational environment)
Shock	5 g's maximum for 45 msec (operational environment) 15 g's maximum for 11 msec (non-operational environment)

A noise temperature analysis was performed on the TASA-II microwave circuit design. A noise temperature model for the new microwave circuit configuration is shown in Figure 7. The following noise temperature analysis is performed on a single channel, and the results are considered typical of all eight channels. The operating temperature (Top) is defined as

$$Top = T_{ant} + T_{sys} \tag{1}$$

where

T_{ant} = antenna noise temperature, and
T_{sys} = antenna system noise temperature.

Using the model in Figure 7, the antenna system noise temperature is

$$T_{sys} = T_o(L_f - 1) + T_{amp} L_f + T_o \frac{(L_s - 1)L_f}{G} + \frac{T_R L_f L_s}{G} \tag{2}$$

where

T_o = 290°K,
L_f = filter insertion and transmission line losses (0.5 dB),
T_{amp} = amplifier noise temperature (84°K),
G = amplifier gain (40 dB),
L_s = system losses following the amplifier, and
T_R = receiver noise temperature (2610°K).

The expected component insertion losses (L_s) are shown in Table III. The noise temperature given by Equation (1) is referenced to the hybrid output terminals (see Figure 7); this location will be used for G/T calculations later. The G/T ratio should remain constant anywhere in the microwave circuit. The antenna noise temperature accounts for noise contribution from ohmic losses in Luneberg lens, hybrid, feed element, and transmission line as well as from the antenna background temperature. The antenna temperature equation is given by

$$T_{ant} = (T_{bg} + T_o (L_a - 1))/L_a \tag{3}$$

where T_{bg} = antenna background temperature, and
L_a = ohmic losses in the antenna.

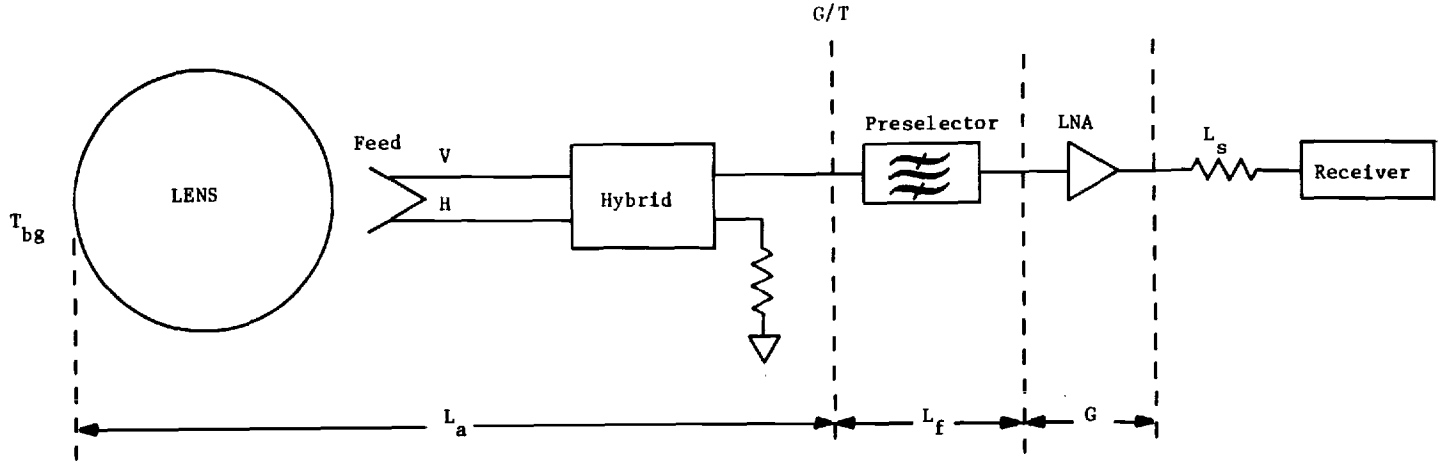

Figure 7. Antenna system noise temperature model.

TABLE III

EXPECTED COMPONENT INSERTION LOSSES

	Insertion Loss (dB)		
Component	Manual/Auto Mode	Two-Beam Combined Mode	Four-Beam Combined Mode
Directional coupler (-10 dB)	0.3	0.3	0.3
SP4T electromechanical switch	0.3	0.3	0.3
2-way combiner	-	0.3	-
4-way combiner	-	-	0.6
PIN-diode switch	2.0	2.0	2.0
coaxial cable (estimate)	1.9	1.9	1.9
Total Estimated Loss	4.5	4.8	5.1

The boresight gain computation for a single beam is given in Table IV. The relatively large spillover loss is due to the small aperture and corresponding broad illumination. Recall that the feed element aperture size was minimized to achieve approximately 3-4 dB beam crossover.

Using Equation (2), the system noise temperature was computed for the manual and automatic modes, and these results are shown in Table V. To properly calculate the noise performance for the two-beam combine and the four-beam combine modes, the noise temperature model must be slightly modified. The two-beam and four-beam combiners serve to sum the single beam responses to generate a broader beam coverage. If these devices were perfect (no insertion losses), then the antenna gain would be reduced and the system noise temperature would remain unchanged. However, the combiners do have ohmic or insertion losses that degrade the system noise performance. Fortunately, the insertion losses for these devices are small and the LNA gain makes their noise contribution negligible. As a result, the noise model must be modified to account for coherent signal summing and non-coherent noise summing. As shown in Table V, system noise temperature changes very little for the two-beam and four-beam combine modes relative to the manual and automatic modes.

TABLE IV

SINGLE BEAM GAIN COMPUTATION AT BORESIGHT

Factor	Budget
$G_o = 4\pi\ A/\lambda^2$ at 2.25 GHz	25.08 dB
Non-Ohmic Losses (Before Filter)	
Spillover	2.0
Element Mismatch	0.2
Radome Mismatch	0.05
	2.25 dB
Ohmic Losses* (Before Filter)	
Luneberg Lens	0.1
Hybrid	0.2
Feed Element	0.1
Transmission Line	0.2
	0.6 dB
Resulting Boresight Gain	22.23 dB

*Negligible radome ohmic loss

Using Equation (3), the antenna noise temperature was computed; the antenna background temperature is a function of several parameters including incidence angle, galactic noise level, solar contribution, and atmospheric absorption. An estimate of 110°K for the antenna noise temperature was established in Reference 3. This value for T_{ant} corresponds to 83°K for T_{bg} using 0.6 dB for L_a (see Table IV). Based on the work of Blake [4], 83°K for T_{bg} can be considered a reasonable value for incidence angles in the range of 0° to 2°. It should be noted that at 0° incidence, this may be a slightly low estimate for T_{bg}; however, T_{bg} is a function of several parameters and conditions that are judged typical by Blake; as a result, T_{bg} is an estimated parameter, and the 110°K for T_{ant} is considered to be a reasonable estimate for these noise temperature calculations based on the range of parameters and conditions that cannot be identified a priori.

The expected G/T for each mode of operation is shown in Table V. The expected antenna gains in the two-beam sum and the four-beam sum modes are based on the expected single beam antenna gain computation shown in Table IV; the gains for the two-beam and four-beam modes are less due to their broader patterns. Assuming a 4 dB beam crossover for both the two-beam and four-beam modes, theoretically (excluding sidelobe contributions) the antenna gains are reduced by 1 dB and 4 dB, respectively.

TABLE V

EXPECTED TELEMETRY NOISE TEMPERATURE AND G/T PERFORMANCE

Antenna Mode	T_{sys} (°K)	T_{op} (°K)	Gain (dB)	G/T (dB/K°)
Auto/Manual	130.1	240.1	22.23	-1.6
Two-beam Combine	130.1	240.1	21.23	-2.6
Four-beam Combine	130.2	240.2	18.23	-5.6

F. Electronic Circuits

1. RF Receivers

The RF receiver design remains unchanged except for several minor modifications. The value for the fixed attenuator used to set the detector log video amplifier (DLVA) dynamic range window is changed. This is due to the different LNA gain used in the TASA-II antenna system. While the LNA gain was reduced to 40 dB, the receiver RF amplifier was increased to 40 dB to provide some compensation to the reduced total RF gain from both amplifiers. See Table VI for the RF amplifier's characteristics. Additional compensation for the gain reduction is accomplished by reducing the fixed attenuator value.

2. Signal Processor and Control Circuits

Modifications to the TASA-II antenna system electronic circuits include the addition of a crowbar on all five bus voltages and the addition of a variable hysteresis loop that changes as a function of the video filter time constant. The crowbar is used to provide over-voltage protection. The power supplies have over-voltage protection; however, the

TABLE VI

RF AMPLIFIER SPECIFICATIONS

Performance	
Frequency Response (min)	2200-2300 MHz
Noise Figure @ 23°C (max)	2.5 dB
Gain (min)	40 dB
Gain Flatness	±0.5 dB
Gain Match (between units) over specified frequency and temperature ranges	1.0 dB
Power Output 1 dB comp. (min)	+7 dBm
Third Order Intercept Point (min)	+20 dBm
VSWR (max) In/Out	2.0:1/1.5:1
Impedance	+50 ohms
Power (max)	+15 VDC @ 60 ma
Connector	SMA Jack
Environmental	
Temperature	0° to 65°C
Humidity	10% to 95% relative
Altitude	0 to 3,000 m
Vibration	1.6 g's maximum for 5 to 55 Hz (operational environment) 3 g's maximum for 55 to 500 Hz (operational environment)
Shock	5 g's maximum for 45 msec (operational environment) 15 g's maximum for 11 msec (non-operational environment)

diodes used to achieve redundancy isolate the power supplies from each other and from the bus. The hysteresis loop circuit in the TASA-I antenna system did not change as a function of filter time constant. As a result, the hysteresis loop threshold levels that initiate beam switching had to be set high enough so that noise on the filtered video signal did not cause false switching regardless of the video filter time constant. Therefore, the old circuit design could not take advantage of the reduced noise on the video signal due to increases in the video filter time constant. It is expected that reducing the trigger threshold when the video filter time constant is increased should improve the receiver sensitivity. Figure 8 presents a conceptual block diagram of the modified control circuits for the TASA-II antenna system. The crowbar and adjustable hysteresis subsystems are identified by dotted lines while the solid lines show the subsystems developed for TASA-I and used in TASA-II.

The design of the electronic circuits for TASA-II adhered to the same design standards used on TASA-I. Satisfactory performance of the TASA-I electronic circuits demonstrate the soundness of the design and changes to the TASA-II electronic circuits are intended to improve its performance relative to TASA-I. Efforts were devoted to keeping: (1) all circuit changes on the same printed circuit board size, and (2) the modified circuit boards pin-for-pin compatible with the circuit boards used in the TASA-I antenna system.

To increase the system reliability and protect the system from overvoltage conditions on the supply buses, a crowbar circuit was added (see Figure 9). As explained earlier, although each power supply has internal overvoltage protection, the diodes used to provide power supply redundancy isolate the internal overvoltage protection from the bus. Therefore, the internal overvoltage protection circuits cannot protect the supply bus. To prevent overvoltage damage, the crowbar will pull the failed supply bus to near ground potential.

Crowbar protection is provided on all five supply buses. If the crowbar is triggered due to overvoltage on any particular bus, both power supplies will attempt to maintain the supply bus at the rated voltage. As a result, a heat sink will be necessary to dissipate heat from the SCRs. This crowbar method is non-destructive; typical crowbar circuits

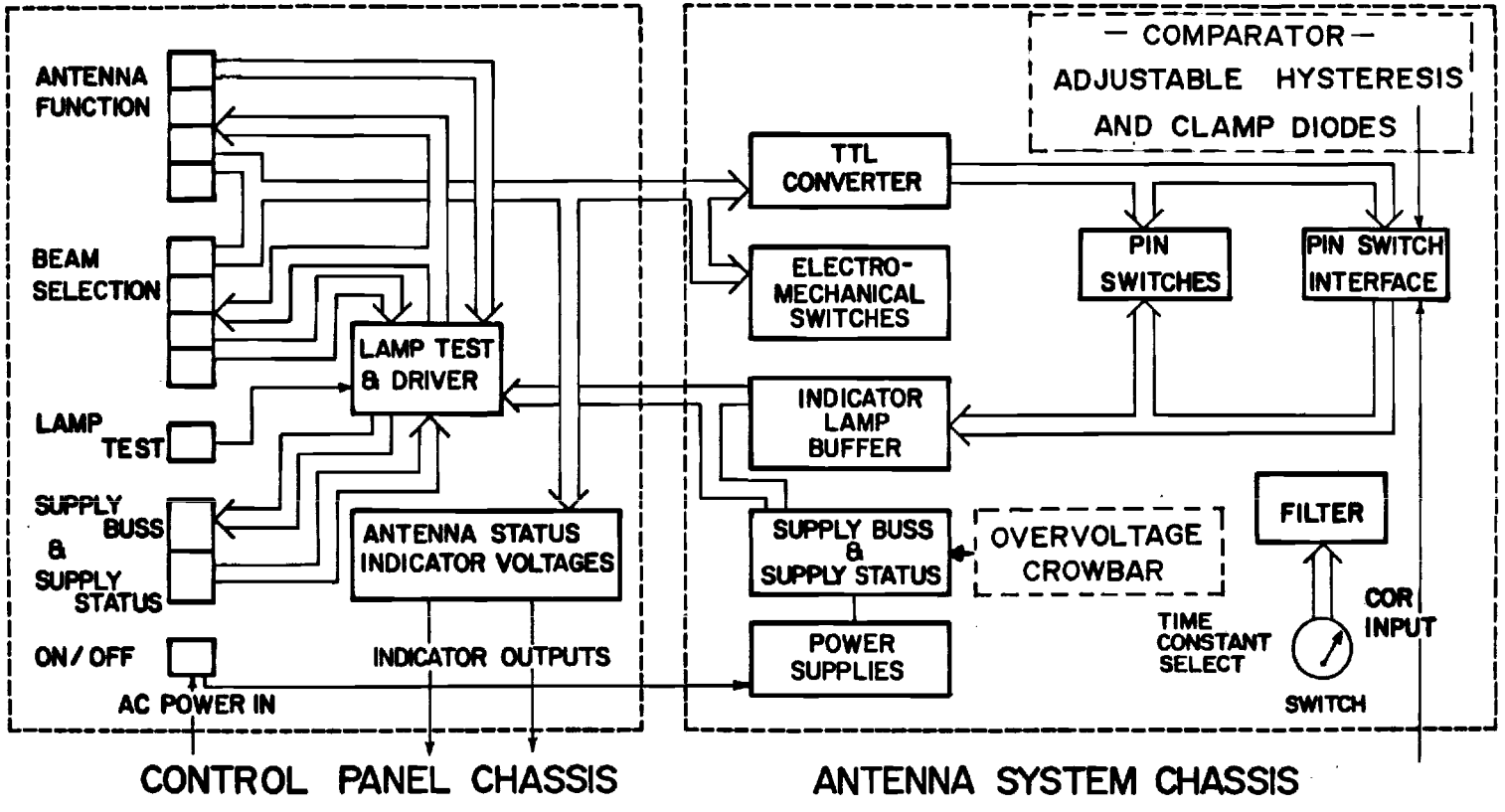

Figure 8. Conceptual block diagram of TASA-II control circuits.

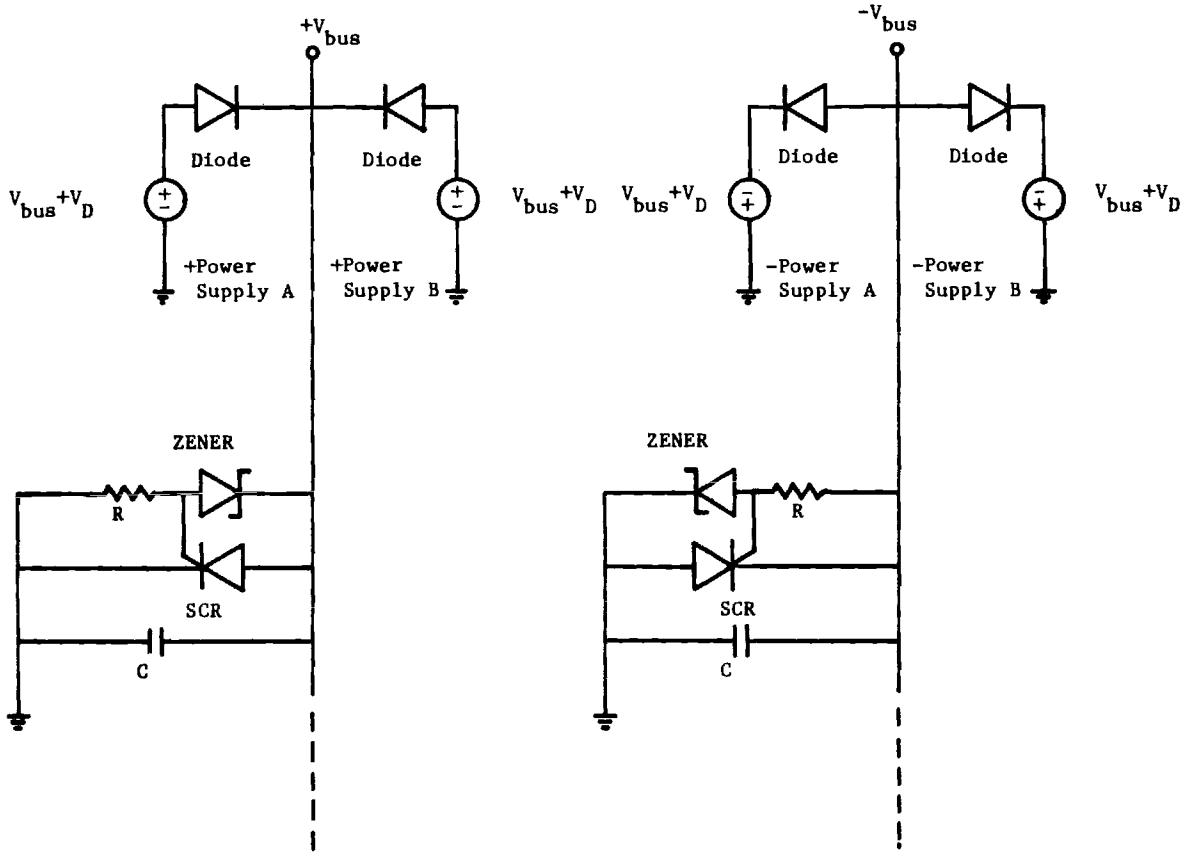

Figure 9. Crowbar circuit diagram for a bipolar power supply.

intentionally blow a fuse when triggered. The fuse must be replaced when the fault is corrected, and a supply of fuses must be maintained. With this crowbar design, once the fault is corrected, the system is again functional without replacing a fuse.

The variable hysteresis circuit is expected to enhance the automatic beam selection process. The noise level at the input of the selection circuitry is a direct function of the signal bandwidth. An improvement in sensitivity could be realized by reducing the hysteresis loop turn-on voltage when the video bandwidth is reduced. Reduced video bandwidth should provide improved sensitivity with a slower response time. The hysteresis is varied by switching different resistor values into the feedback loop of the hysteresis circuit by means of a CMOS protected analog switch. The CMOS switch is controlled by the same switch that controls the filter time constant.

SECTION III

ANTENNA SYSTEM FABRICATION AND TESTING

A. Introduction

The TASA-II antenna system was fabricated like the TASA-I antenna system except for those design changes described in Section II. This section of the report will discuss the implementation of these modifications; in addition, measured system performance data are presented in this section.

B. Mechanical Assembly

The entire mechanical structure is fabricated from aluminum alloys (6061-T6 and 5052-H32). The basic structure is assembled with rivet fasteners, and stainless steel screws with floating inserts are used on all removable cover plates. The new feed carriage assembly is the primary mechanical modification to the antenna system. This structure is pictured in Figure 10. As previously discussed, the feed carriage assembly can be completely removed from the mechanical structure, and stainless steel guide pins facilitate removal with accurate replacement. In addition to the easy removal of the feed carriage assembly, the LNAs and preselect filters can be easily removed from the feed carriage assembly.

In order to protect against moisture and electromagnetic interference, RFI gasket materials were used on all compartments with removable panels. The access panels and control panel were labeled using a silkscreen process with a high wear resistance ink, and several coats of clear polyurethane sealer were applied for additional protection. After completion of the TASA-II antenna system, its weight was approximately 160 lbs. This is only an increase of about 4 lbs. over the TASA-I antenna, and it is due to the additional weight from the improvements made to the TASA-II antenna system.

C. Radome Assembly

Radome Serial Number 100 was used in the TASA-II antenna. Previous tests [2] showed that it was the best of the two remaining Luneberg lenses. Recall that this lens had to be reoriented to improve its electrical performance. It was rotated approximately 45° clockwise (viewed from the

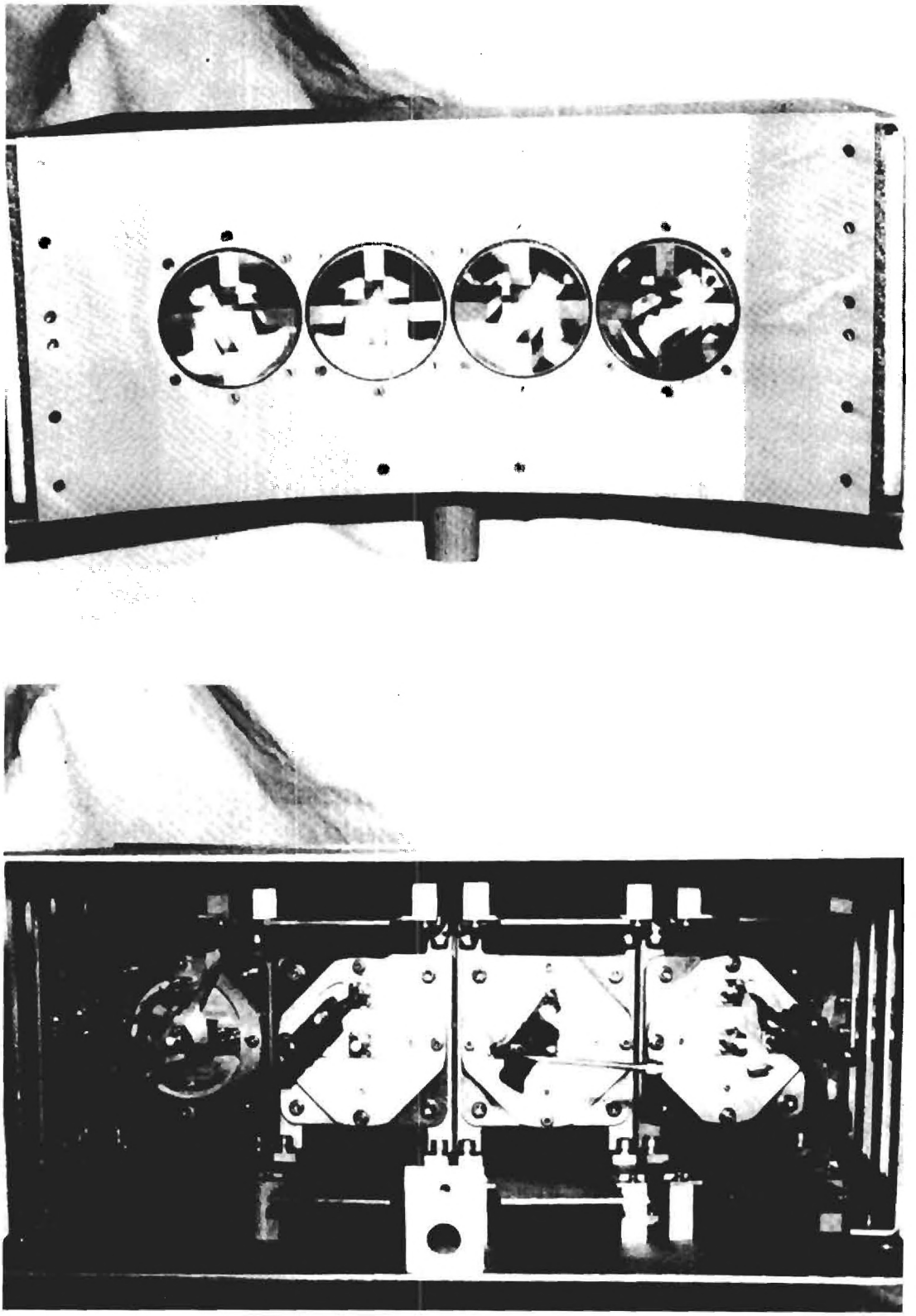

Figure 10. Front (top) and rear (bottom) photographs of the feed carriage assembly.

front) in the polar plane. The fiberglass mounting ring was redrilled to mount the lens in this prefered orientation.

D. Antenna RF Feeds

The fabrication of the antenna feed element used in the TASA-I antenna system remains unchanged except for the feed element end plate. A picture of the new coax-to-waveguide adapter with the modified end plate is shown in Figure 11. In the center of the modified end plate, a mounting surface for the electrically small RF probe has been added. The probe was fabricated from a SMA bulkhead connector (CDI 5220CCSF). Reference channel insertion loss data using the RF probes are presented in Section III-G.

E. Microwave Circuitry

The microwave circuit described in Section II-E was constructed with 0.141 semi-rigid cable. Most of these transmission lines were phase balanced over the 2.2-2.3 GHz frequency range with the aid of a automated network analyzer. Specifically, any signal path from the feed elements to either the two-way combiner or the four-way combiner required phase balancing of the transmission lines. All microwave circuit signal paths were tested over the 2.2-2.3 GHz frequency range to insure proper operation. In addition, microwave circuit active and passive components were tested to document compliance with specification; particular attention was paid to the LNAs and low-loss (preselect) bandpass filters. Observe that the three character code described in Section II-E is used to label all eight channels. Test data on the microwave circuitry are presented in Section III-G.

A dip in the four-beam sum mode antenna response was experienced in the TASA-I system; it is due to destructive interference from the exterior beam's first sidelobes (beams R2 and L2). The sidelobes add out-of-phase to produce a dip in the middle of the four-beam sum mode antenna response. The pattern response was reshaped by changing the relative phasing between feed elements. Instead of summing all four feed elements in phase in the four-way combiner, the exterior beams (R2 and L2) are about 45° out-of-phase relative to the interior beams (R1 and L1). Pattern measurements presented later in this section (see Section III-G) demonstrate that this

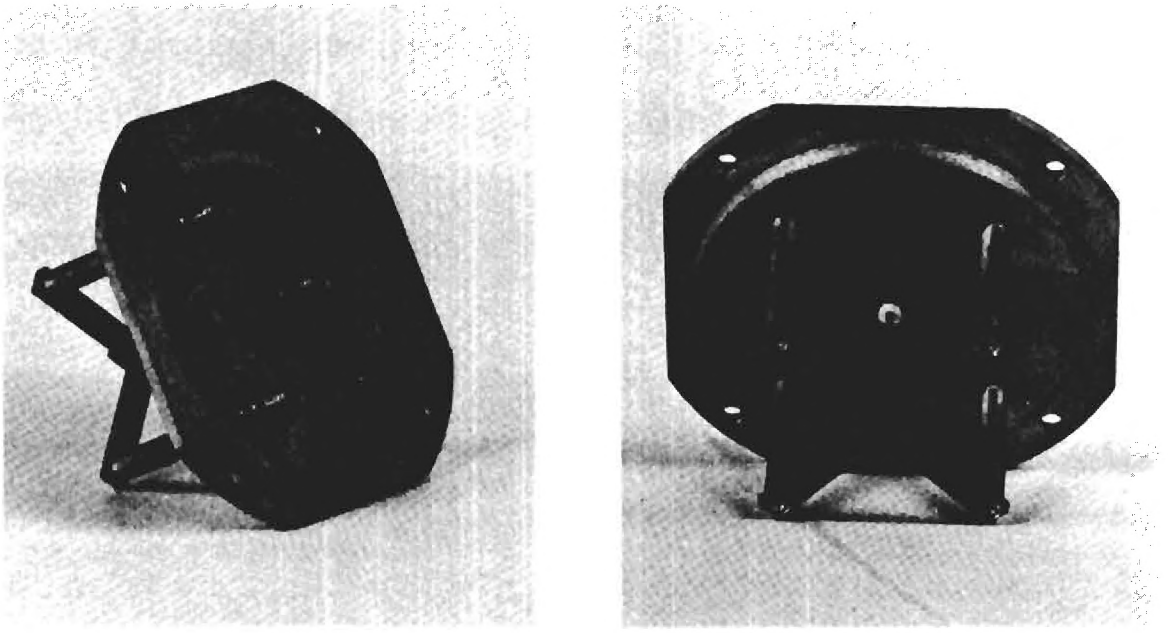

a) New coax-to-waveguide adapter

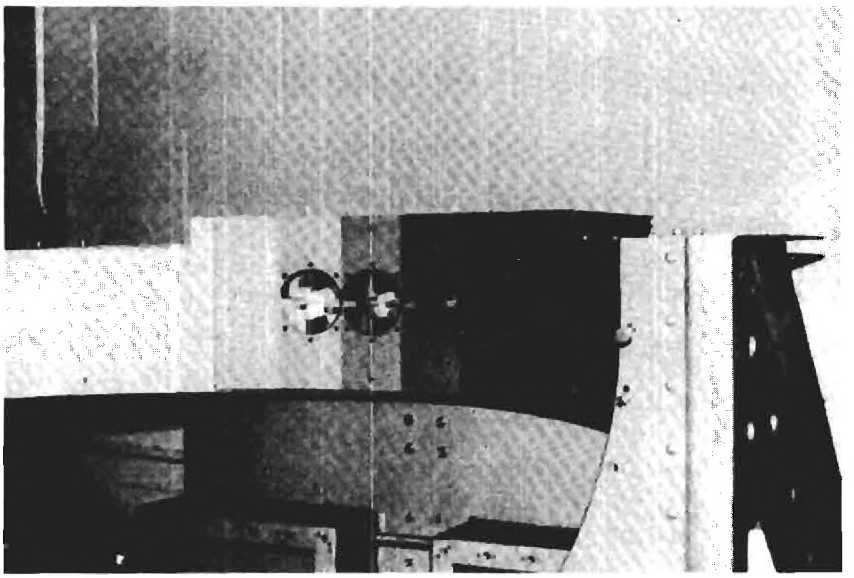

b) Four element array

Figure 11. Photographs of the new coax-to-waveguide adapter with the reference signal injection probe (a) and the four element array mounted in the mechanical structure (b).

technique significantly reduced the magnitude of the dip in the four-beam sum mode pattern response.

F. Electronic Circuitry

1. RF Receivers

Eight RF receivers were built into the antenna system according to the diagram presented in Figure 12. Mounting of the receivers in the mechanical assembly was changed to facilitate maintenance and reduce the number of semi-rigid cables. All receiver components were tested to establish proper performance relative to the specification. Recall that the RF amplifier gain was increased to 40 dB relative to the RF amplifiers used in the TASA-I antenna system. Due to the reduction in combined gain from the LNA and RF amplifiers, different fixed attenuator values were needed to set the dynamic range window of the DLVA. Notice from Figure 12 that 6 dB fixed attenuators were used on the input and output of the RF amplifier. In addition to controlling the dynamic range window of the DLVA, these attenuators also improved the RF amplifier isolation. In order to improve the amplifier's noise rejection and expected sensitivity, the tubular RF bandpass filter is located between the amplifier output and the input to the DLVA. The amount of attenuation from the fixed attenuators (12 dB total per channel) places the amount of RF amplification at about the same level as used in the TASA-I antenna system.

RF receiver sensitivity tests were performed to establish the RF signal level at which the electronic beam switching circuitry would initiate a command to switch to the appropriate channel. These tests were performed for video bandwidths of 10 Hz and 1,000 Hz with corresponding measured sensitivities of -110 dBm and -105 dBm, respectively. These sensitivity levels are an improvement over the switching levels observed in the TASA-I antenna system, and the improved sensitivities are attributable to the modified hysteresis circuit. This modified circuit changes trigger threshold levels when the video filter bandwidth is switched from 100 Hz to 1000 Hz; note that both 10 Hz and 100 Hz video filter bandwidths use the same threshold while 1000 Hz and 10,000 Hz video filter bandwidths use the same threshold.

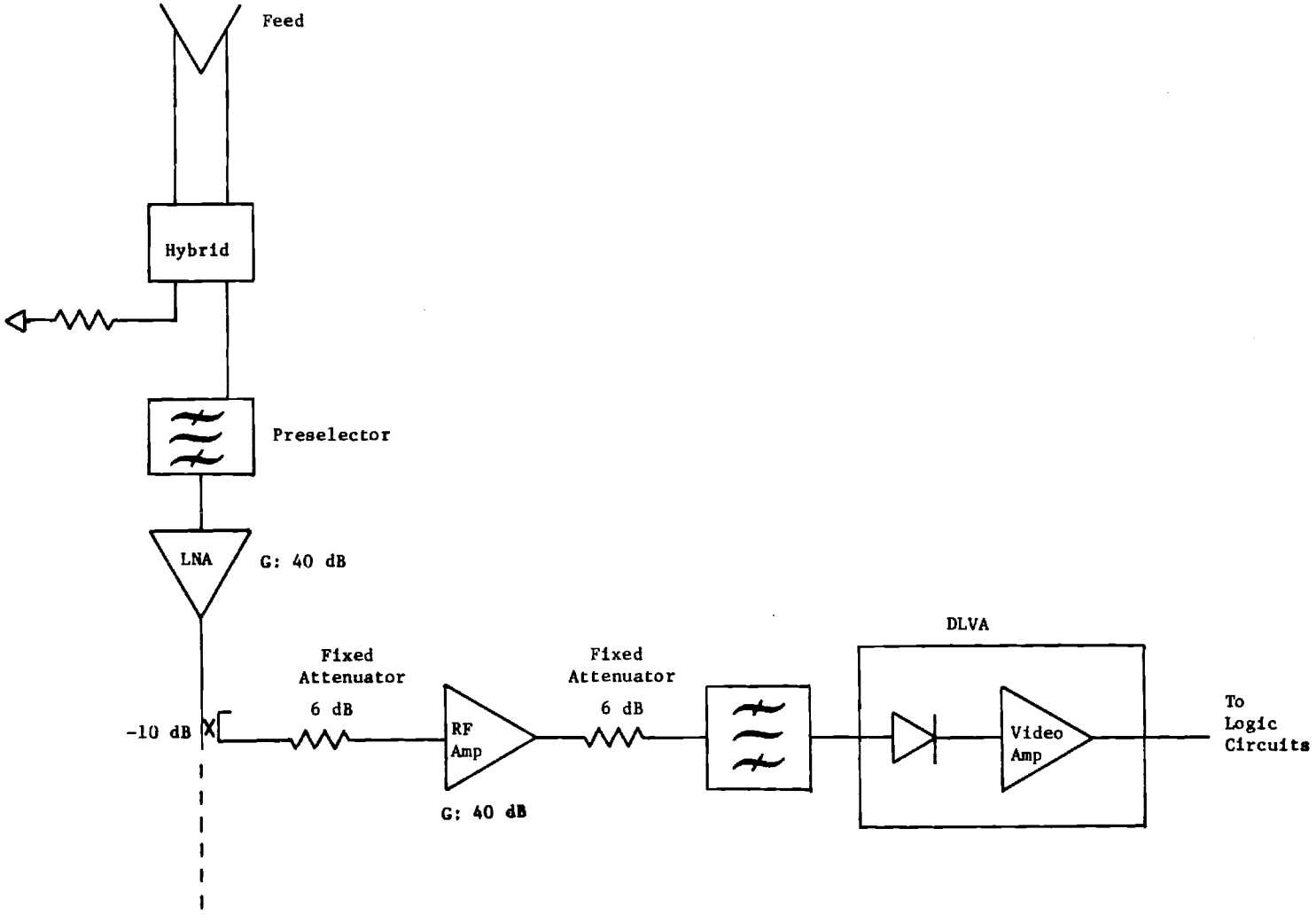

Figure 12. Block diagram of TASA-II receiver.

2. Signal Processor and Control Circuits

This section of the report describes the implementation of modifications to the automatic beam selection and control circuits. Recall that in the TASA-I antenna system, all electronic circuits were contained in three circuit boards. These circuit boards were referred to as the automatic circuit board, the manual circuit board, and the control panel circuit board. The automatic circuit board controls the beam selection process in the automatic beam selection mode. The control panel circuit board has circuits that control the antenna system and the indicator lights on the front control panel. The manual circuit board controls the antenna in the manual modes of operation; these are the two-beam sum mode, the four-beam sum mode, and the manual beam select mode. The manual and automatic circuit boards are shown in the electronics compartment in Figure 13.

These three circuit boards are each fabricated on a S-100 size printed circuit board with plated through holes. The control panel circuit board and the manual circuit board were unmodified relative to the TASA-I system; however, the automatic circuit board was modified to include the adjustable hysteresis loop. Care was taken in the printed circuit board layout so that all circuit modifications were limited to the standard size S-100 circuit board. Initially, it was planned to add the crowbar circuit to the existing manual circuit board; in fact, the circuit board layout provides for the crowbar circuit. But in order to provide a better heatsink, the crowbar circuit was built on its own circuit board and mounted on a larger heatsink. When the crowbar is activated, the bus indicator light on the control panel will go off, and the system must be turned off and the fault corrected before the crowbar circuit will recycle. Tests on the crowbar circuit demonstrate its capability to provide prolonged protection without component failure. The circuit diagrams for these printed circuit boards are shown in Figures 14-17. The antenna wiring and the control panel wiring diagrams are shown in Figures 18-19. The circuit board and system wiring diagrams are in Appendix I. To facilitate reading this document, all remaining figures are presented in the appropriate appendix.

G. Antenna System Test Results

This section gives the results of measurements performed on the

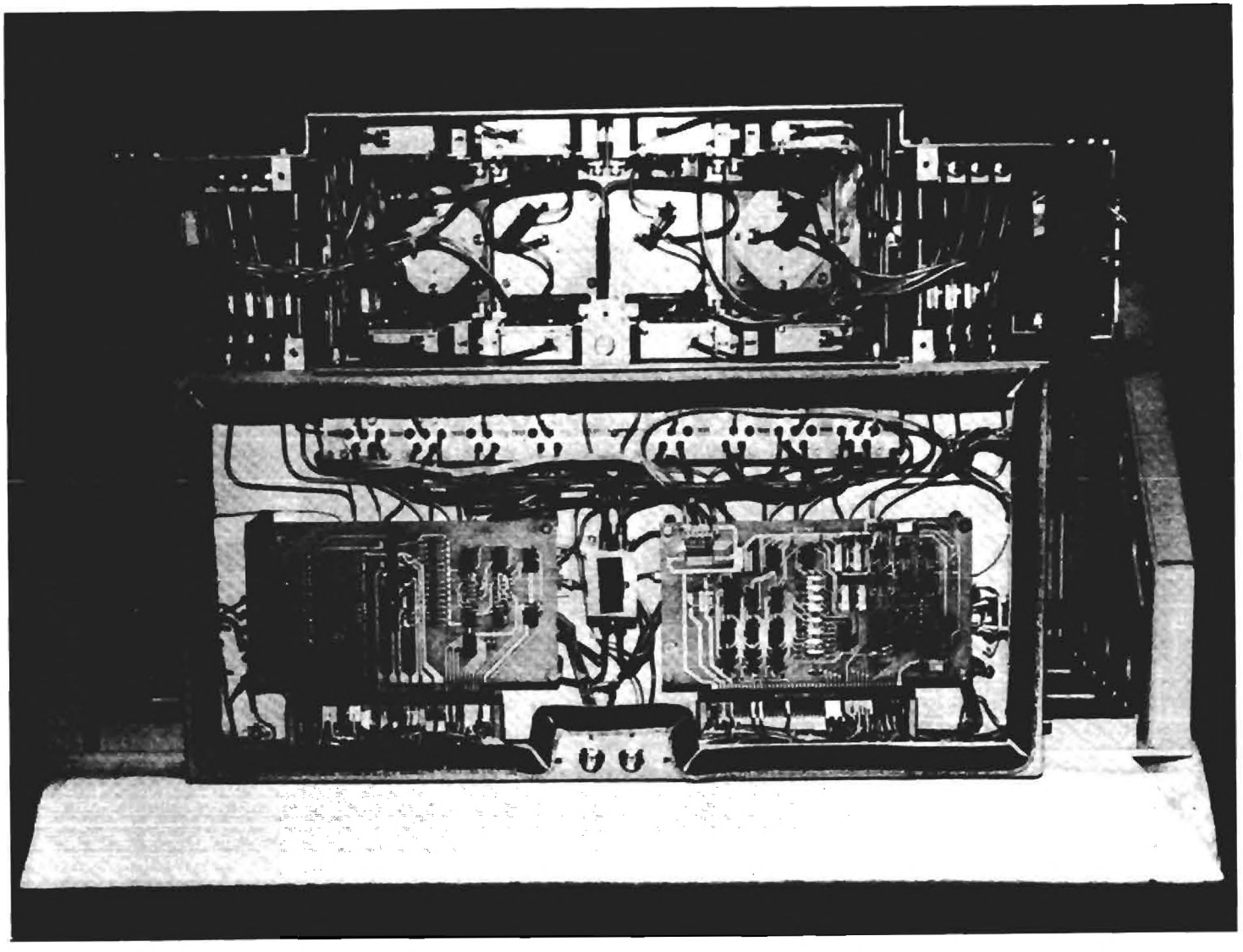

Figure 13. Rear photograph of antenna system with access panels removed.

antenna system to establish its compliance with the specifications. Data presented include: (1) noise figure measurements, (2) system insertion gain measurements, (3) reference channel insertion loss measurements, (4) antenna pattern data, and (5) G/T calculations.

The system noise figure measurements are shown in Table VII. These measurements were made between the low-loss preselect filter input and the antenna system output ports. Notice from Table VII that measurements were performed on all eight channels. In addition, these measurements were obtained with an AILTECH precision automatic noise figure indicator (Model No. 7514) with appropriate mixers, RF source, and noise source (Model No. 7618). The noise source was calibrated against a cryogenic termination at 2.25 GHz. Notice that the average noise figure for all channels is 1.35 dB. This measured value should closely correspond to the calculated value of T_{sys} given in Table V. The only difference is that the calculations included the noise contribution from the TM receiver. The noise measurements do not include the receiver in the system; however, the LNA gain is sufficiently large so that the receiver noise contribution is negligible, and the measured and calculated values for T_{sys} should closely compare regardless of the TM receiver. The primary reason for the lower measured noise figure is due to the lower noise figure of the delivered LNAs. All LNAs built for the TASA-II antenna system had noise figures between 0.75 dB and 0.9 dB.

TABLE VII

SYSTEM NOISE FIGURE MEASUREMENTS

Channel	Noise Figure (dB)
R1L	1.25
R2L	1.35
L1L	1.30
L2L	1.40
L2R	1.45
L1R	1.40
R1R	1.30
R2R	1.35

Swept-frequency system insertion gain measurements are presented in Figure 20 (see Appendix II). This test was performed between the low-loss preselect filter input ports and the system output ports. Data were taken for the antenna in the manual mode, two-beam combine mode, and the four-beam combine mode. The measurements were made using an appropriate signal source and scalar network analyzer (Wiltron Model No. 560).

Reference channel insertion loss measurements are presented in Figure 21 (see Appendix II). This test was performed between the referenced channel input port and appropriate hybrid right- and left-hand-circular output ports. These measurements were obtained using a scalar network analyzer (Wiltron Model No. 560) and an appropriate signal source.

Extensive antenna pattern measurements were obtained from the assembled TASA-II antenna system on the compact range at Georgia Tech. The compact range field was probed to insure proper alignment and establish the characteristics of the plane wave. This facility is capable of both fixed and rotating linear polarized radiation; rotation of the source polarization is a useful method to measure the response of a circularly polarized antenna.

The antenna patterns presented in Figures 22-44 (see Appendix III) are from the comprehensive set of pattern measurements performed on this antenna. The patterns show the antenna response to both fixed linear polarization (FLP) and rotating linear polarization (RLP). The mainbeam pattern response to RLP in both the azimuth and elevation principal planes for the antenna in the automatic, manual, two-beam sum, and four-beam sum modes are shown in Figures 22-36. Notice that the antenna response shown in these patterns is much better behaved than comparable patterns from TASA-I; the TASA-II axial ratio is now 2-3 dB. The antenna response, including the sidelobes, is shown in Figures 37-44 to FLP; these patterns present azimuth and elevation principal plane data for both vertical and horizontal polarizations. The antenna gain relative to linear isotropic is labeled on each of the patterns and this gain reference was accomplished with a standard gain horn. The standard gain horn is linearly polarized and its response was inserted in the antenna system's microwave circuitry at the low-loss preselect filter input port (see Figure 6).

The antenna system gain relative to circular polarization can be obtained using several relationships described in Reference 1. The antenna axial ratio (AR) is defined as

$$AR = \frac{E_{min}}{E_{max}} \tag{4}$$

where $-1 \leq AR \leq 1$,
E_{min} = minimum response to rotating linear polarization, and
E_{max} = maximum response to rotating linear polarization.

Observe those figures that show the pattern response to RLP; values for E_{max} and E_{min} as well as the axial ratio can be obtained directly from these measurements. With the axial ratio and peak gain information, the antenna gain relative to circular polarization can be obtained by

$$G_{RHC} = G_{LHC} = G_{max} + 10 \log \frac{(1+|AR|)^2}{2} \tag{5}$$

where G_{RHC} = antenna gain relative to right-hand-circular polarization,
G_{LHC} = antenna gain relative to left-hand-circular polarization, and
G_{max} = peak antenna gain relative to linear polarization.

Notice from Equation (5) that when AR is unity ($E_{max} = E_{min}$), the antenna gain relative to either right- or left-hand-circular polarization is 3 dB above the antenna gain relative to linear polarization. Using Equation (5), the average antenna gain (relative to circular) is 22.5 dBci, 21.5 dBci, and 18.2 dBci for the manual and automatic modes, two-beam sum mode, and four-beam sum mode, respectively.

The antenna system G/T calculations are presented in Table VIII. The antenna gains relative to circular isotropic were taken from the previously discussed antenna patterns. In addition, the antenna system operating temperature (T_{op}) is based upon the measurements for T_{sys} and the estimated 110°K for T_{ant}. Therefore, using an average value of 1.35 dB for T_{sys}, T_{op} is 216°K. Because the antenna system noise temperature is essentially the telemetry system noise temperature (due to the LNA gain), these G/T data should reflect the G/T for the telemetry system. The results presented in

Table VIII compare well with calculations given in Table V. Based on the calculated G/T shown in Table VIII, the antenna system exceeded the G/T design goals.

In addition to these tests, miscellaneous electrical measurements were performed to insure proper antenna performance prior to shipment. The antenna status indicator output voltages functioned properly, and the antenna system power requirements were the same as TASA-I, about 200 watts.

TABLE VIII

ANTENNA SYSTEM G/T CALCULATIONS

Mode	Average Gain (dBci)*	Top (°K)	G/T (dB/°K)
Manual/Auto	22.5	216	-0.8
Two-beam Sum	21.5	216	-1.8
Four-beam Sum	18.2	216	-5.1

*includes both G_{RHC} and G_{LHC}.

SECTION IV

CONCLUSIONS AND RECOMMENDATONS

This report has described the successful efforts by Georgia Tech personnel to improve the TASA antenna system. Each design modification has resulted in improved antenna system performance. These modifications and resulting performance were discussed in Sections II and III of this report. The improvements include: (1) better axial ratio performance, (2) easier antenna system maintenance, (3) direct reference signal injection for calibration purposes, (4) RF preselect filters for LNA protection, (5) RF diagnostic output ports, (6) crowbar circuit, and (7) selectable hysteresis loop circuit. The antenna system axial ratio is now 2-3 dB regardless of either antenna mode or frequency of operation. The maintenance of the entire antenna system has been simplified; the feed carriage assembly is completely removable from the mechanical structure and LNAs can be easily removed from the feed carriage assembly. Additional system protection has been provided with crowbar circuits on all bus voltages. All of these modifications to the TASA-II antenna system only increased its weight about four pounds over the TASA-I antenna system. The total weight for the TASA-II antenna system is approximately 160 lbs. All RF receivers have a minimum sensitivity of -99 dBm, and the antenna system noise temperature (T_{sys}) without the data receiver averages 1.35 dB.

The TASA-II antenna system contains many of the same features as the TASA-I antenna system. The antenna has both instantaneous left- and right-hand-circular polarized outputs and is designed to operate in the 2.2-2.3 GHz frequency range with four selectable modes of operation. These modes are: (1) a manual mode, where all four feeds can be individually selected, (2) a two-beam combine mode where the two interior feeds are coherently summed, (3) a four-beam combine mode, where all four feeds are coherently summed, and (4) an automatic mode, where any feed can be automatically selected by electronics depending upon which beam contains the largest signal. Antenna system control and status monitoring is remotely accomplished from a rack mounted panel. This control panel provides for antenna mode selection and antenna beam selection in the manual mode. Indicator lights identify the selected antenna mode as well as which

antenna feed is active. In addition, indicator lights show the status of the antenna system power supplies and bus voltages.

The recommendations as a result of this program are two-fold. First (and of primary importance), the TASA-I antenna system should be modified to match the performance of the TASA-II antenna system. Second, the control panel circuit board should be modified to provide beam selection information in the automatic mode.

SECTION V

REFERENCES

1. W. P. Cooke, et al, "Design, Fabrication, and Test of the S-Band TASA Telemetry Antenna System," Georgia Institute of Technology, Final Technical Report, Project A-3028, Purchase Order No. K110915-X (Prime Contract DASG60-76-C-0002), July 1982.

2. W. P. Cooke, "Test and Analysis of the TASA Luneberg Lens Antenna," Georgia Institute of Technology, Final Technial Report, Project A-3288, Purchase Order No. K151026-XH (under Government Prime DASG60-82-C-002), February 1983.

3. "Caribou TASA Study," Kwajalein Missile Range Directorate, Ballistic Missile Defense System Command, Huntsville, Alabama, 23 October 1980.

4. L. V. Blake, "A Guide to Basic Pulse-Radar Maximum-Range Calculation," NRL Report 6930, 23 December 1969.

APPENDIX I

CIRCUIT BOARD AND SYSTEM WIRING DIAGRAMS

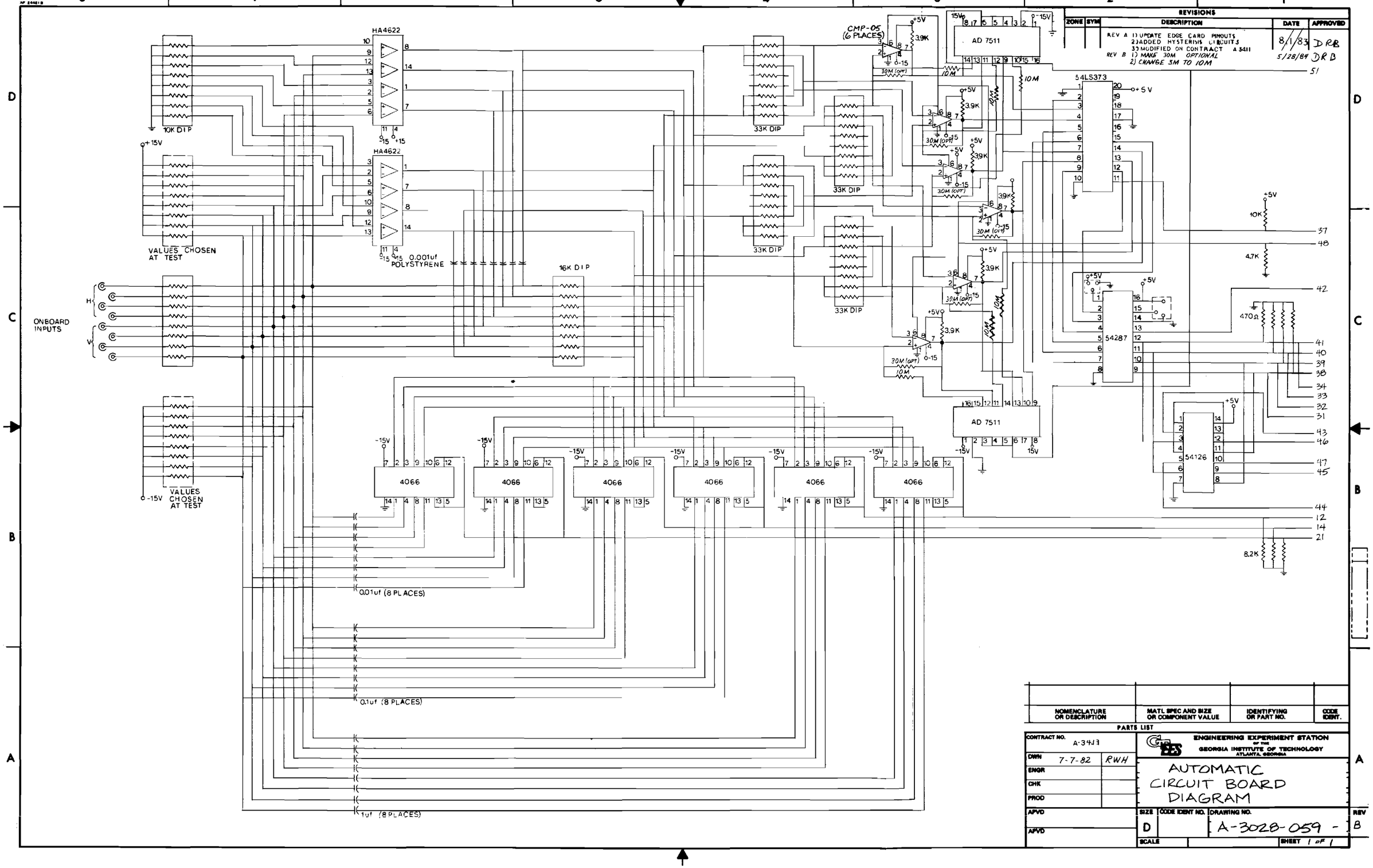

Figure 14. Automatic circuit board diagram.

APPLICATION			REVISIONS				
QTY REQD	NEXT ASSY	USED ON	ZONE	SYM	DESCRIPTION	DATE	APPROVED
					REV A 1) UPDATE WIRING 2) MODIFIED COLOR CODE 3) MODIFIED ON CONTRACT A3411	8/1/83	DRB

L2 L1 R1 R2

SUPPLY BUSS LAMP TEST

M A 2B 4B

2BEAM 4BEAM AUTO MAN. ANT.10 ANT.20 ANT.30 ANT.40 SUPPLIES BUSS GND. +28V +5V +15V -15V -5V ANT.4L ANT.3L ANT.2L ANT.1L

V_{O_1} V_{O_2}

KEY

GRAY-A LAMP-L
BROWN-B
BLUE-C
GREEN-D
WHITE-E
BLACK-F
VIOLET-G
ORANGE-H
RED-I
YELLOW-J
BURGUNDY-K

ITEM OR FIND NO.	QTY REQD	NOMENCLATURE OR DESCRIPTION	MATL SPEC AND SIZE OR COMPONENT VALUE	IDENTIFYING OR PART NO.	CODE IDENT.

PARTS LIST

ALL DIMENSIONS ARE IN INCHES UNLESS OTHERWISE SPECIFIED
TOLERANCES
3 PLACE DECIMALS ±
2 PLACE DECIMALS ±
1 PLACE DECIMAL ±
FRACTIONS ± ANGLES ± 0°30'
MAX SURFACE ROUGHNESS 125 ALL MACHINED SURFACES EXCEPT AS NOTED
BREAK SHARP EDGES AND CORNERS .010 MAX
FINISH

CONTRACT NO. A 3411
DWN 7-7-82 RWH
ENGR
CHK
PROD
APVD
APVD

ENGINEERING EXPERIMENT STATION OF THE GEORGIA INSTITUTE OF TECHNOLOGY ATLANTA, GEORGIA

CONTROL PANEL WIRING DIAGRAM

SIZE D | CODE IDENT NO. | DRAWING NO. A-3028-060- | REV A

SCALE | SHEET 1 OF 1

Figure 19. Control panel chassis wiring harness diagram.

APPLICATION			REVISIONS				
QTY REQD	NEXT ASSY	USED ON	ZONE	SYM	DESCRIPTION	DATE	APPROVED
					REV A 1) UPDATE EDGE CARD PINOUT 2) MODIFIED ON CONTRACT A 3411	8/1/83	DRB
					REV B 1) UPDATE CROWBAR CIRCUIT, ADD SUBHEADING	5-30-84	DRB

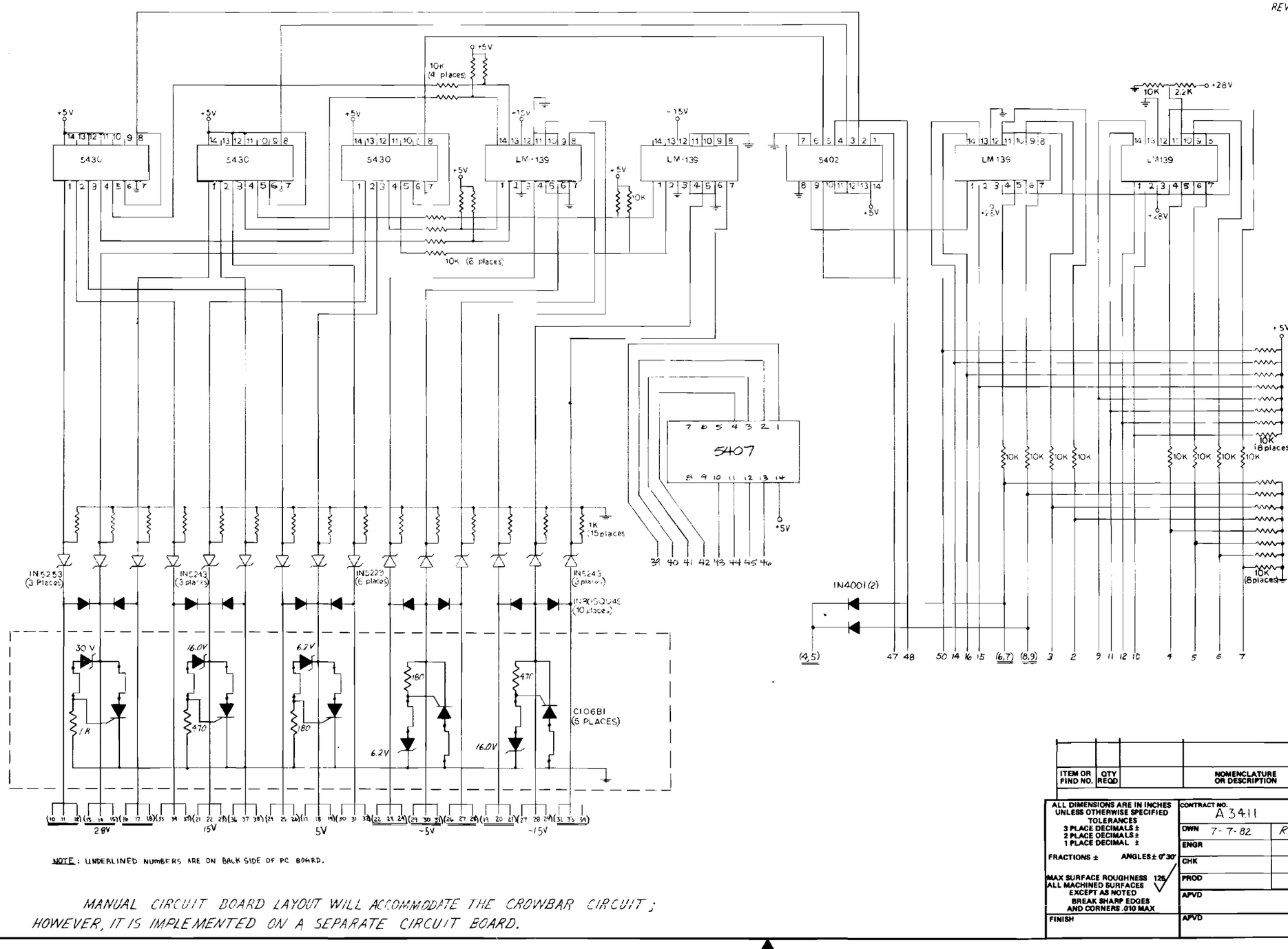

NOTE: UNDERLINED NUMBERS ARE ON BACK SIDE OF PC BOARD.

MANUAL CIRCUIT BOARD LAYOUT WILL ACCOMMODATE THE CROWBAR CIRCUIT; HOWEVER, IT IS IMPLEMENTED ON A SEPARATE CIRCUIT BOARD.

ITEM OR FIND NO.	QTY REQD	NOMENCLATURE OR DESCRIPTION	MATL SPEC AND SIZE OR COMPONENT VALUE	IDENTIFYING OR PART NO.	CODE IDENT.

PARTS LIST

ALL DIMENSIONS ARE IN INCHES UNLESS OTHERWISE SPECIFIED
TOLERANCES
3 PLACE DECIMALS ±
2 PLACE DECIMALS ±
1 PLACE DECIMAL ±
FRACTIONS ± ANGLES ± 0°30'
MAX SURFACE ROUGHNESS 125 ALL MACHINED SURFACES EXCEPT AS NOTED BREAK SHARP EDGES AND CORNERS .010 MAX
FINISH

CONTRACT NO. A 3411
DWN 7-7-82 RWH
ENGR
CHK
PROD
APVD
APVD

ENGINEERING EXPERIMENT STATION OF THE GEORGIA INSTITUTE OF TECHNOLOGY ATLANTA, GEORGIA

MANUAL CIRCUIT BOARD DIAGRAM

SIZE D | CODE IDENT NO. | DRAWING NO. A-3028-061- | REV B
SCALE | SHEET 1 of 1

Figure 15. Manual circuit board diagram.

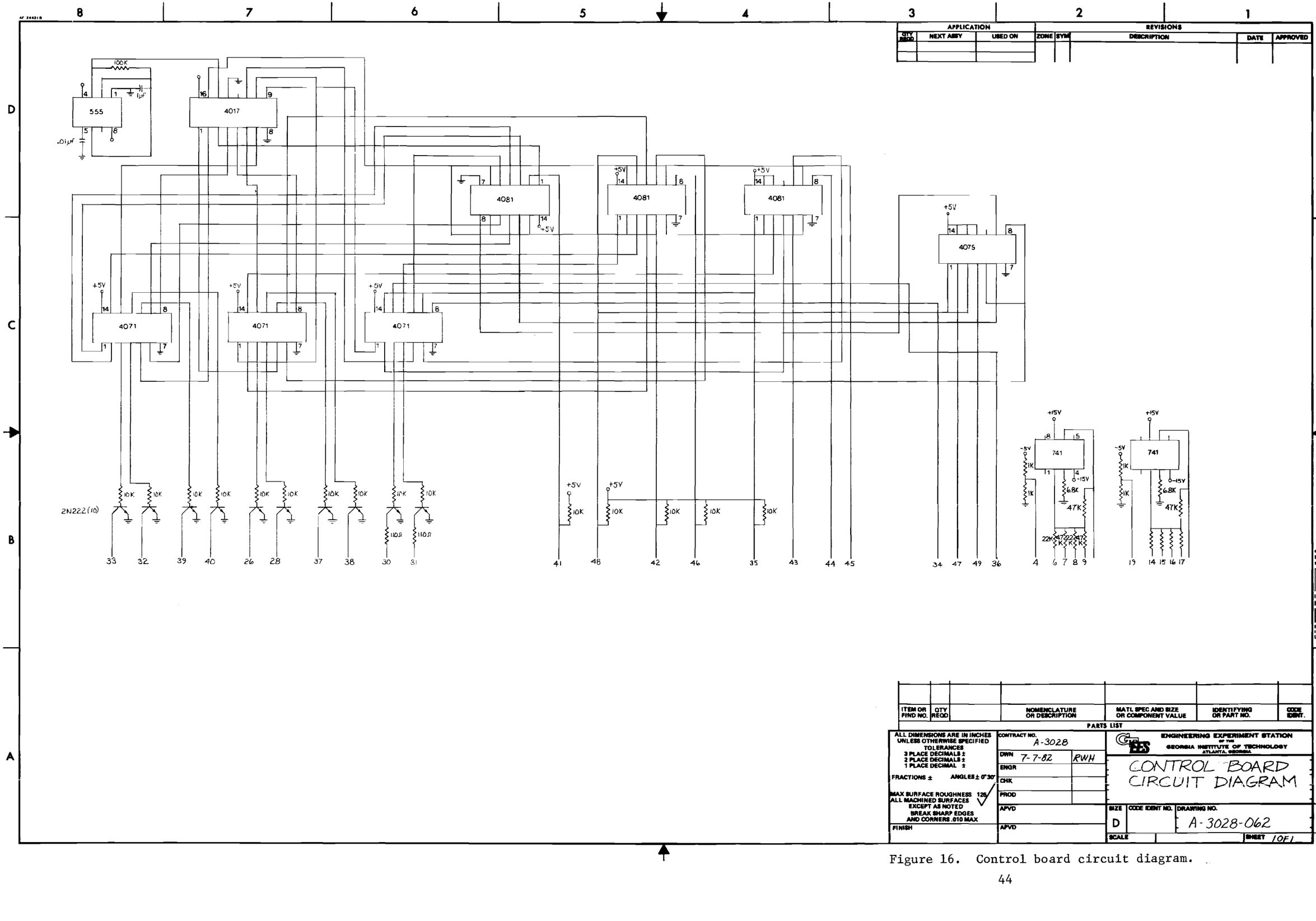

Figure 16. Control board circuit diagram.

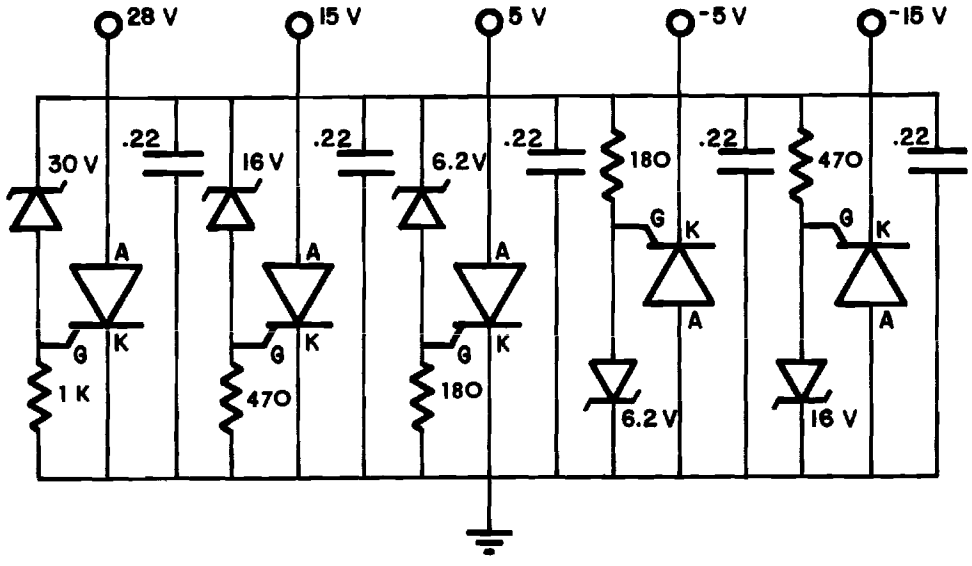

Figure 17. Crowbar board circuit diagram.

APPLICATION			REVISIONS			
QTY REQD	NEXT ASSY	USED ON	ZONE	SYM	DESCRIPTION	DATE	APPROVED
					REV A 1) MODIFIED COLOR CODE 2) MODIFIED ON CONTRACT A 3411	8/1/83	DRB
					REV B 1) ADDED CROWBAR CIRCUIT	5-31-84	DRB

POWER SUPPLY A — +28 +15 +5 -5 -15 — G I H K J

POWER SUPPLY B — +28 +15 +5 -5 -15 — G I H K J

CROWBAR CIRCUIT — +28 +15 +5 -5 -15

TEST — G

OPERATE — F

1P6T R.F. MECH SWITCHES — CENTER PIN, TEST, AUTO/MAN, 4BEAM, 2BEAM — F, B, B, A

PIN SWITCHES — 4BEAM, 2BEAM, ANT4, ANT3, ANT2, ANT1, +5V, -5V — J, H, J, Q, C, F, A, G

A 25	2 BEAM	d
B	4 BEAM	b a Z
C	AUTO	Y K
20		W
B	MAN	V
D	ANT1	U
C	ANT2	T
A	ANT3	S
E 15	ANT4	R
B	SUPPLIES	P
D	BUSS	N M
F	GND	L
10		K
G	+28V	J
H	+5V	H
I	+15V	G
J	-15V	F
K 5	-5V	E
E	ANT4	D
A	ANT3	C
C	ANT2	B
D 1	ANT1	A

B COR

T4a T4b D
B T3a T3b
B T2a T2b
B T1a T1b
F C C

+5V +15V -15V -5V -28V

1 10 20 30 40 50

KEY
GREY - A
BROWN - B
BLUE - C
GREEN - D
WHITE - E
BLACK - F
VIOLET - G
ORANGE - H
RED - I
YELLOW - J
BURGUNDY - K
VIOLET WHITE - L
BROWN WHITE - M

ITEM OR FIND NO.	QTY REQD	NOMENCLATURE OR DESCRIPTION	MATL SPEC AND SIZE OR COMPONENT VALUE	IDENTIFYING OR PART NO.	CODE IDENT.

PARTS LIST

ALL DIMENSIONS ARE IN INCHES UNLESS OTHERWISE SPECIFIED
TOLERANCES
3 PLACE DECIMALS ±
2 PLACE DECIMALS ±
1 PLACE DECIMAL ±
FRACTIONS ± ANGLES ± 0°30'
MAX SURFACE ROUGHNESS 125 ALL MACHINED SURFACES EXCEPT AS NOTED BREAK SHARP EDGES AND CORNERS .010 MAX
FINISH

CONTRACT NO. A-3411

DWN	7-7-82	RWH
ENGR		
CHK		
PROD		
APVD		
APVD		

ENGINEERING EXPERIMENT STATION OF THE GEORGIA INSTITUTE OF TECHNOLOGY ATLANTA, GEORGIA

ANTENNA WIRING DIAGRAM

SIZE	CODE IDENT NO.	DRAWING NO.	REV
D		A-3028-063	B

SCALE — SHEET 1 OF 1

Figure 18. Antenna system chassis wiring harness diagram.

APPENDIX II

SWEPT-FREQUENCY MEASUREMENTS

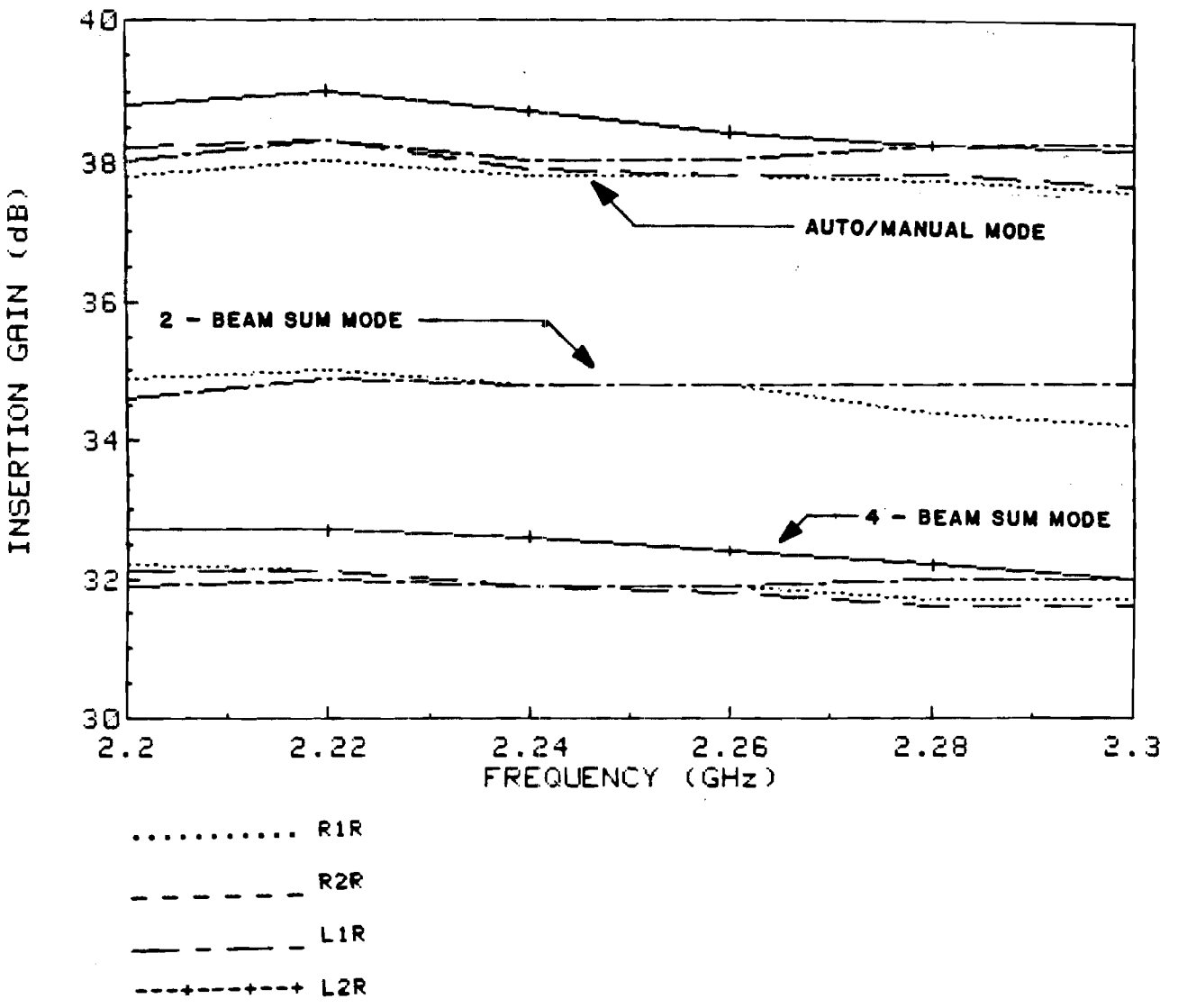

Figure 20. Swept-frequency system insertion gain measurements (continued).

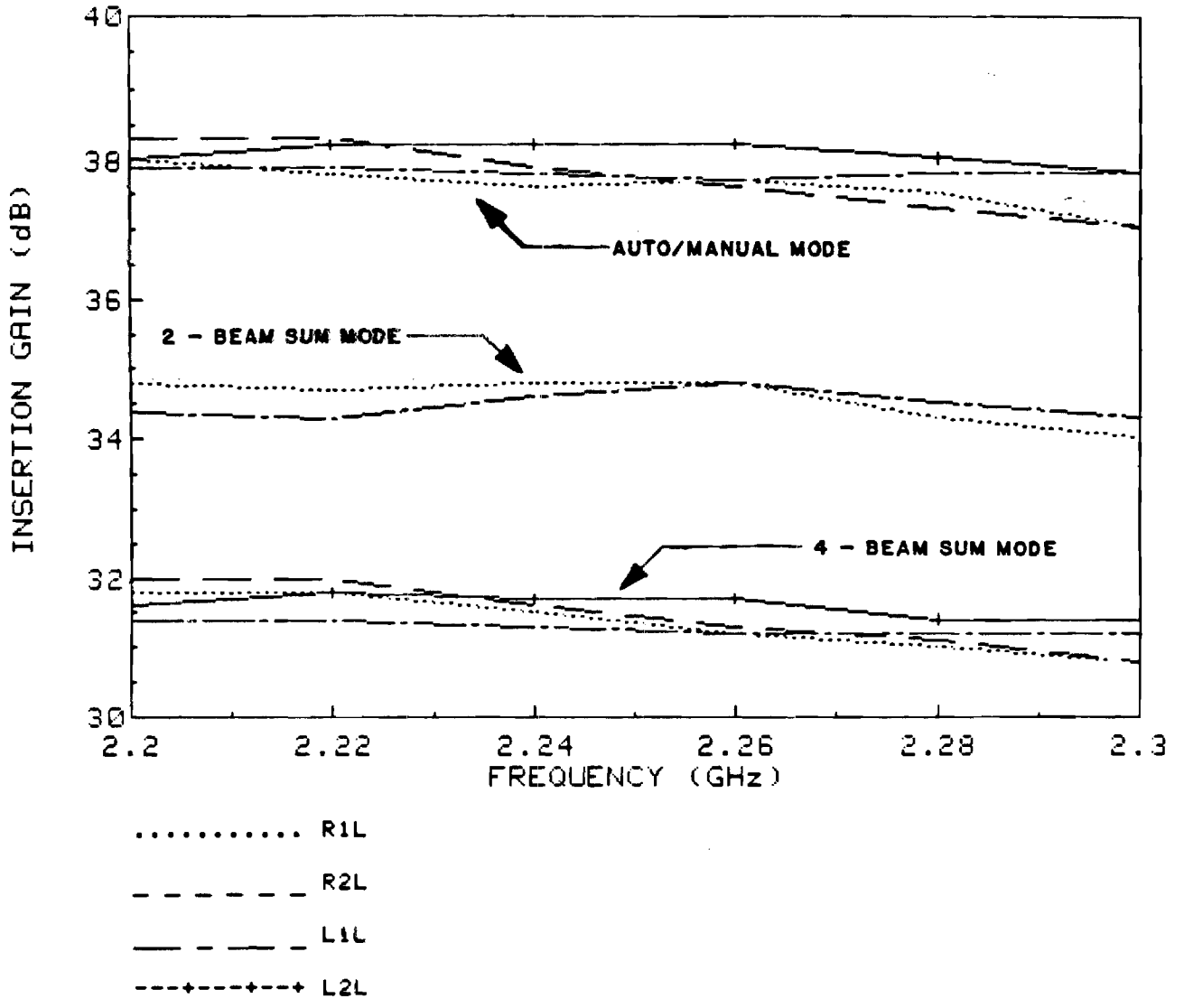

Figure 20. Swept-frequency system insertion gain measurements.

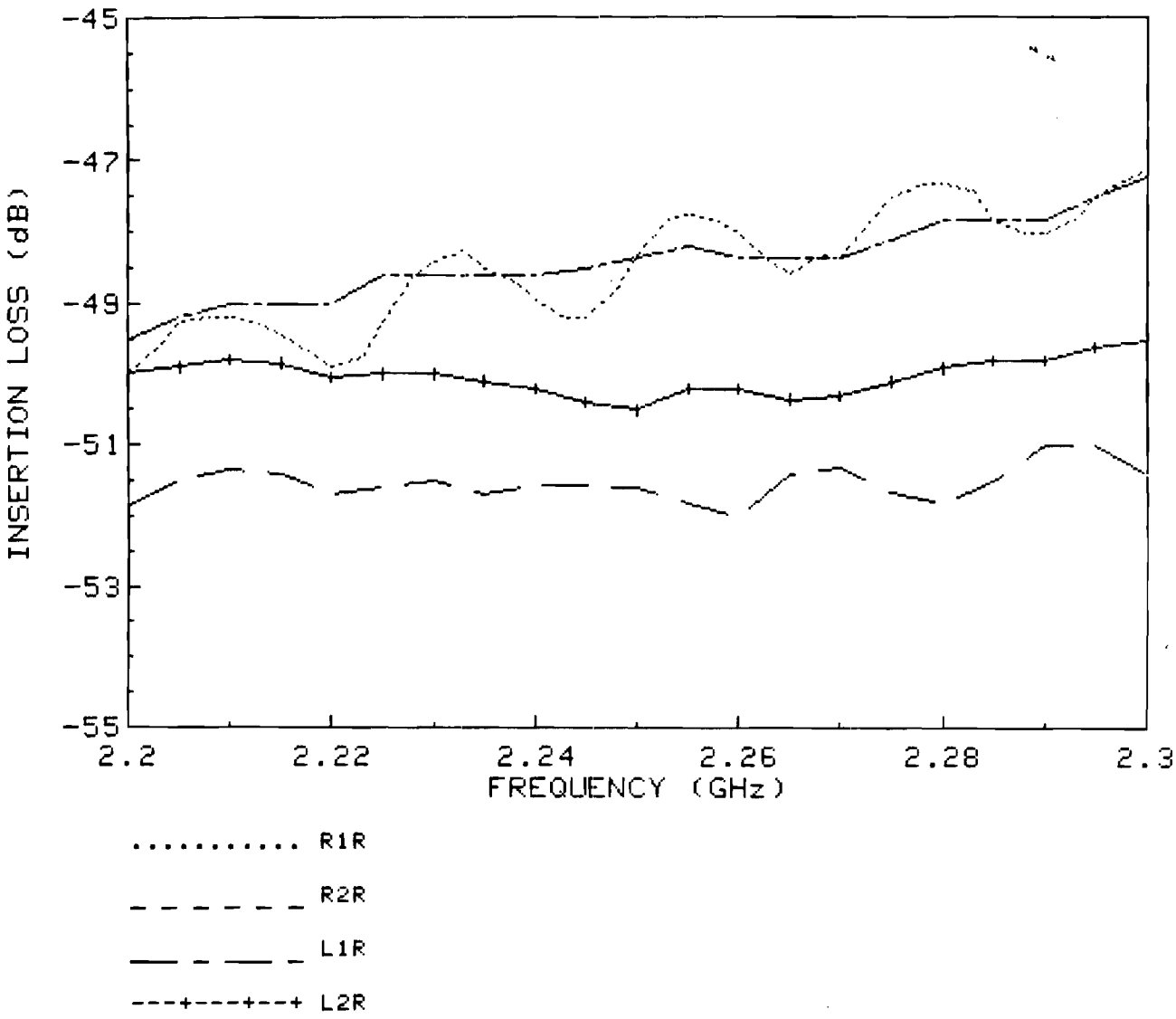

Figure 21. Swept-frequency reference channel insertion loss measurements (continued).

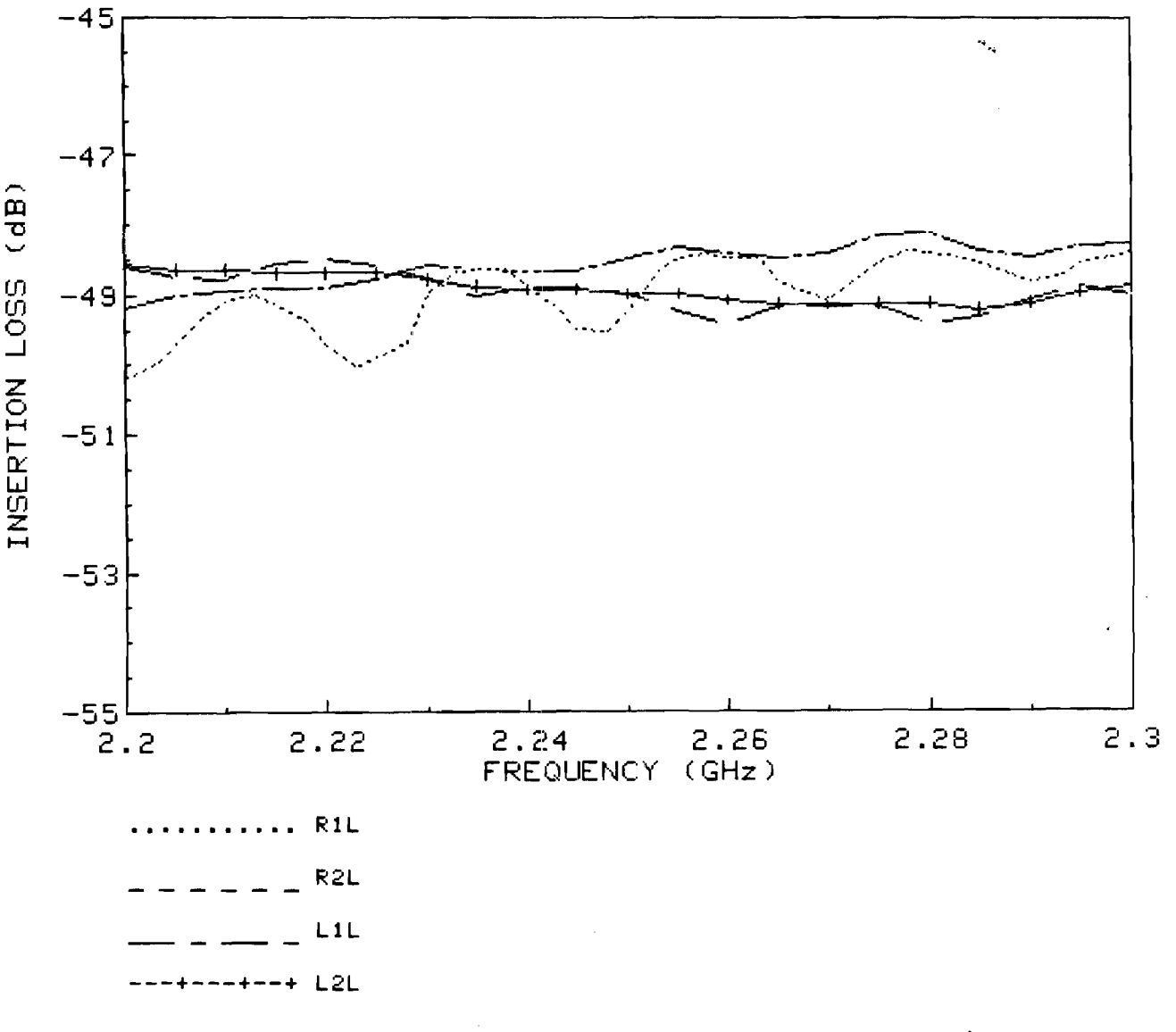

Figure 21. Swept-frequency reference channel insertion loss measurements.

APPENDIX III

SELECTED TASA-II ANTENNA PATTERNS

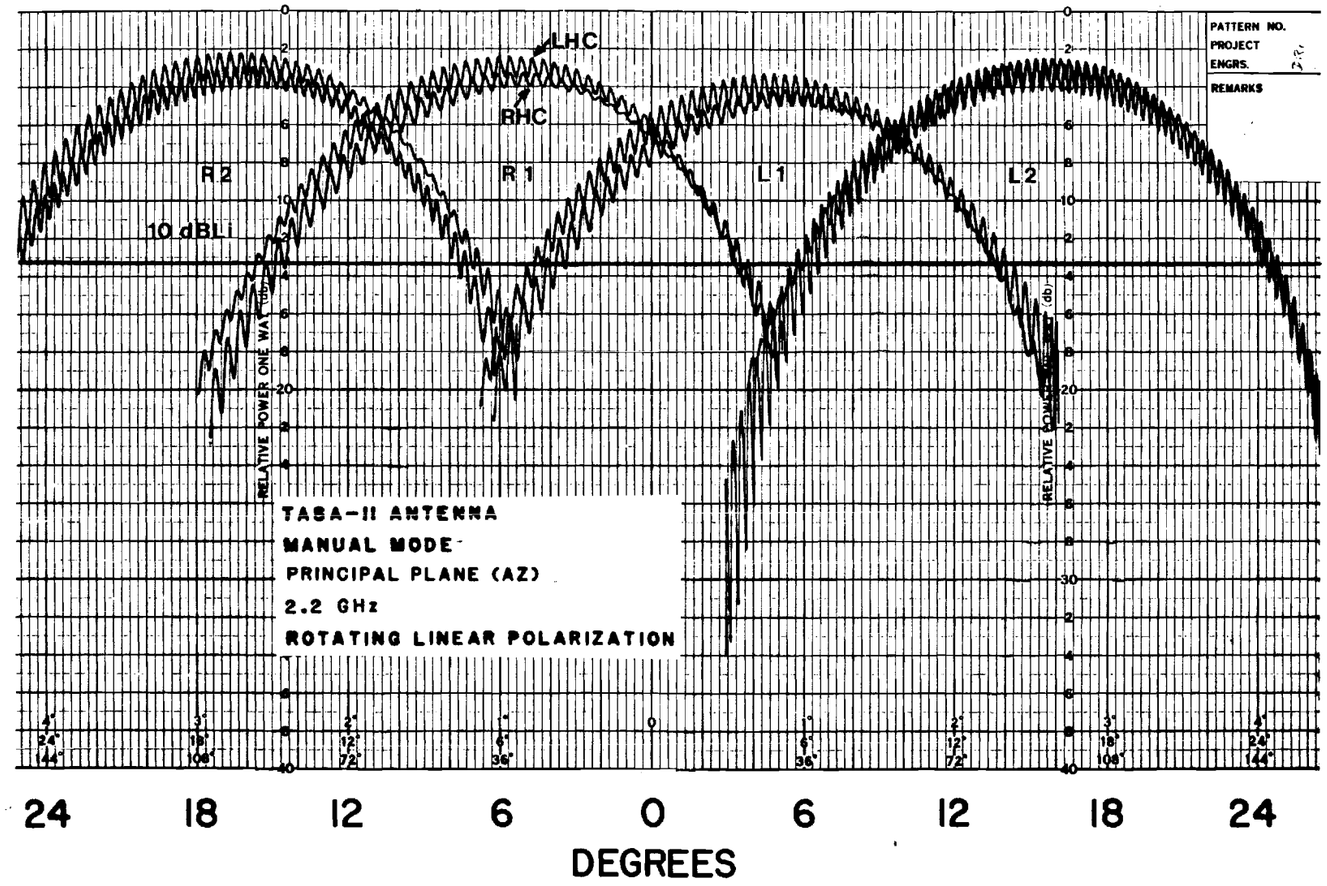

Figure 22. Principal plane (AZ) pattern (RLP) at 2.2 GHz in the manual mode.

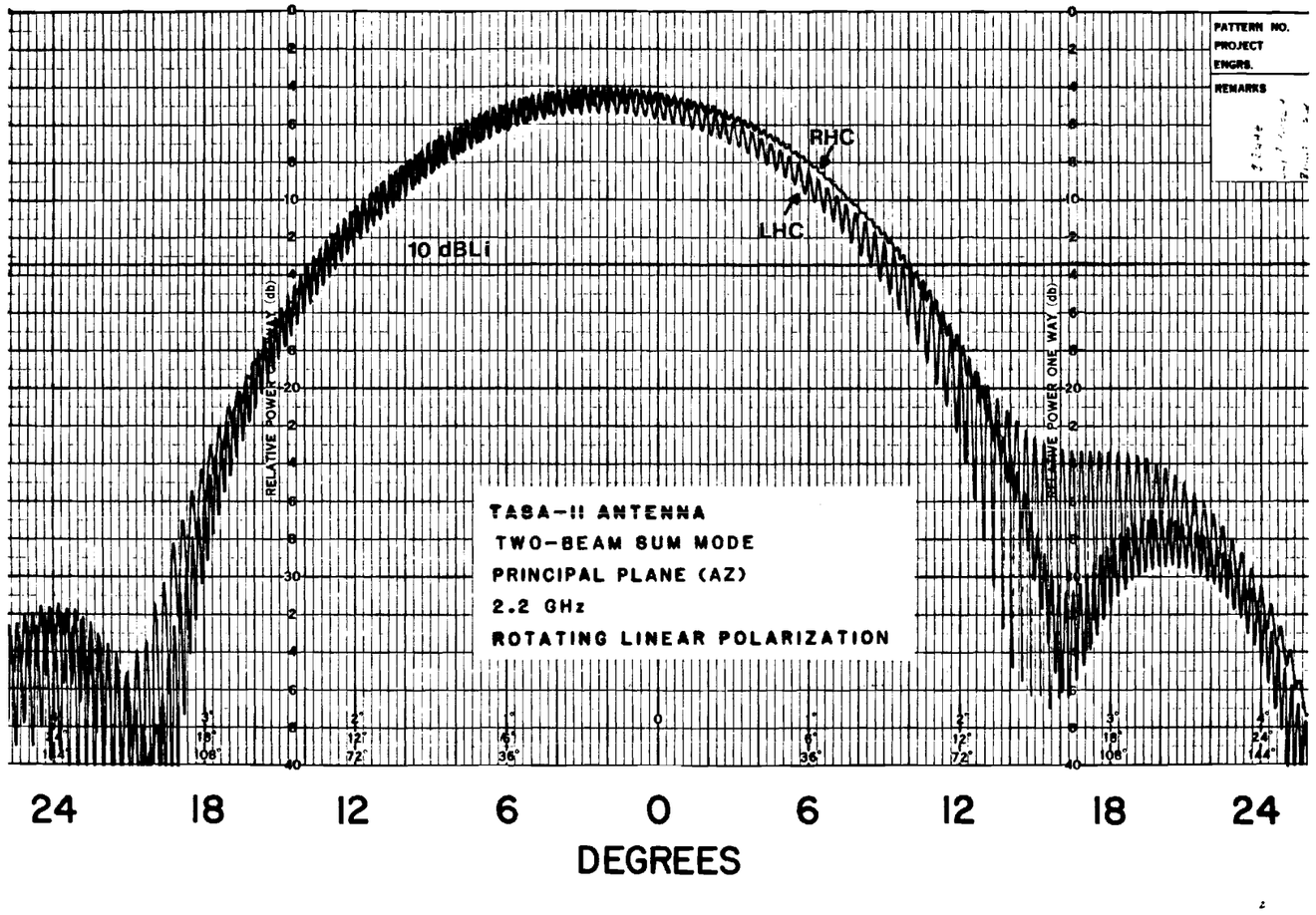

Figure 23. Principal plane (AZ) pattern (RLP) at 2.2 GHz in the two-beam sum mode.

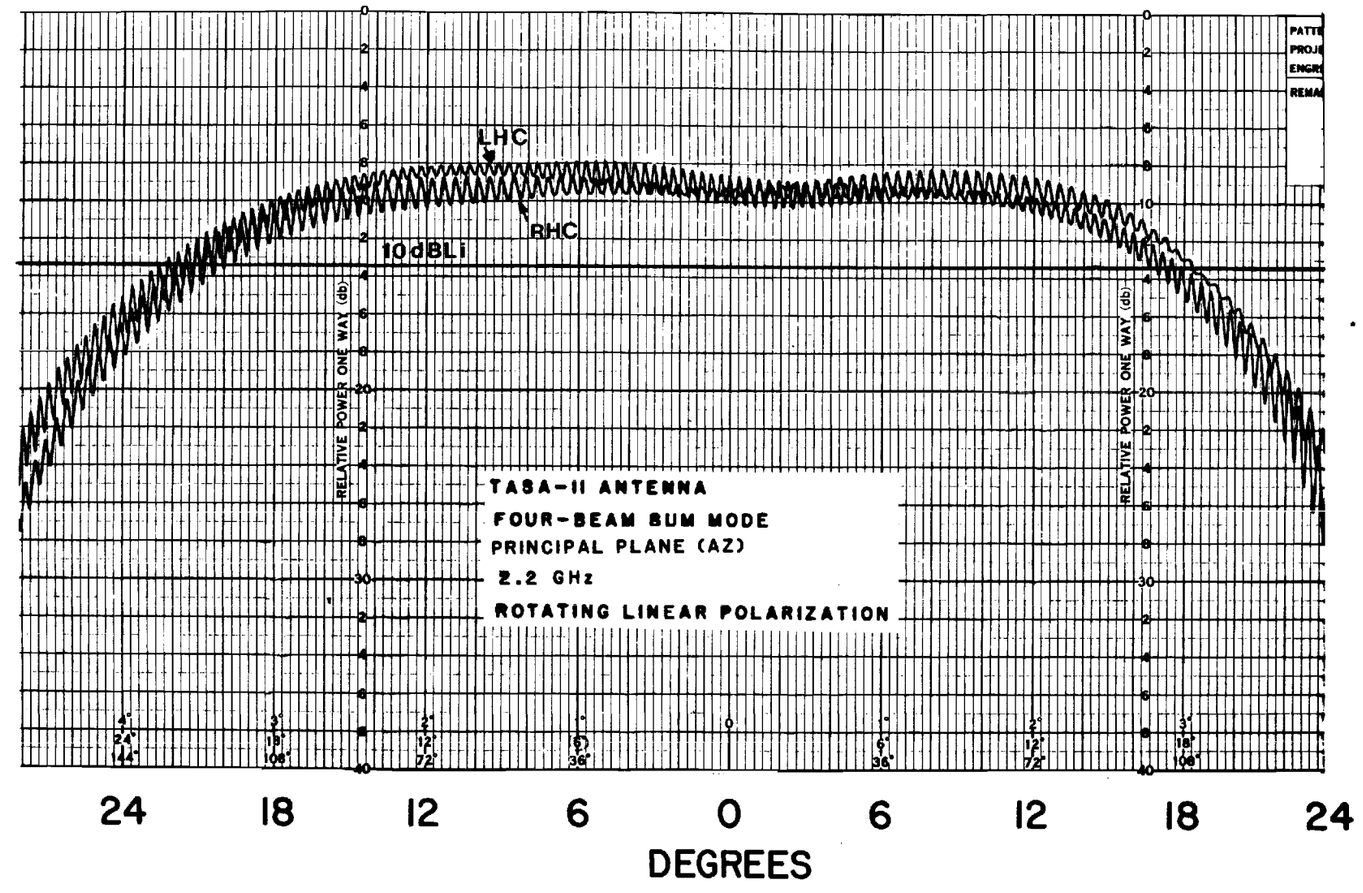

Figure 24. Principal plane (AZ) pattern (RLP) at 2.2 GHz in the four-beam sum mode.

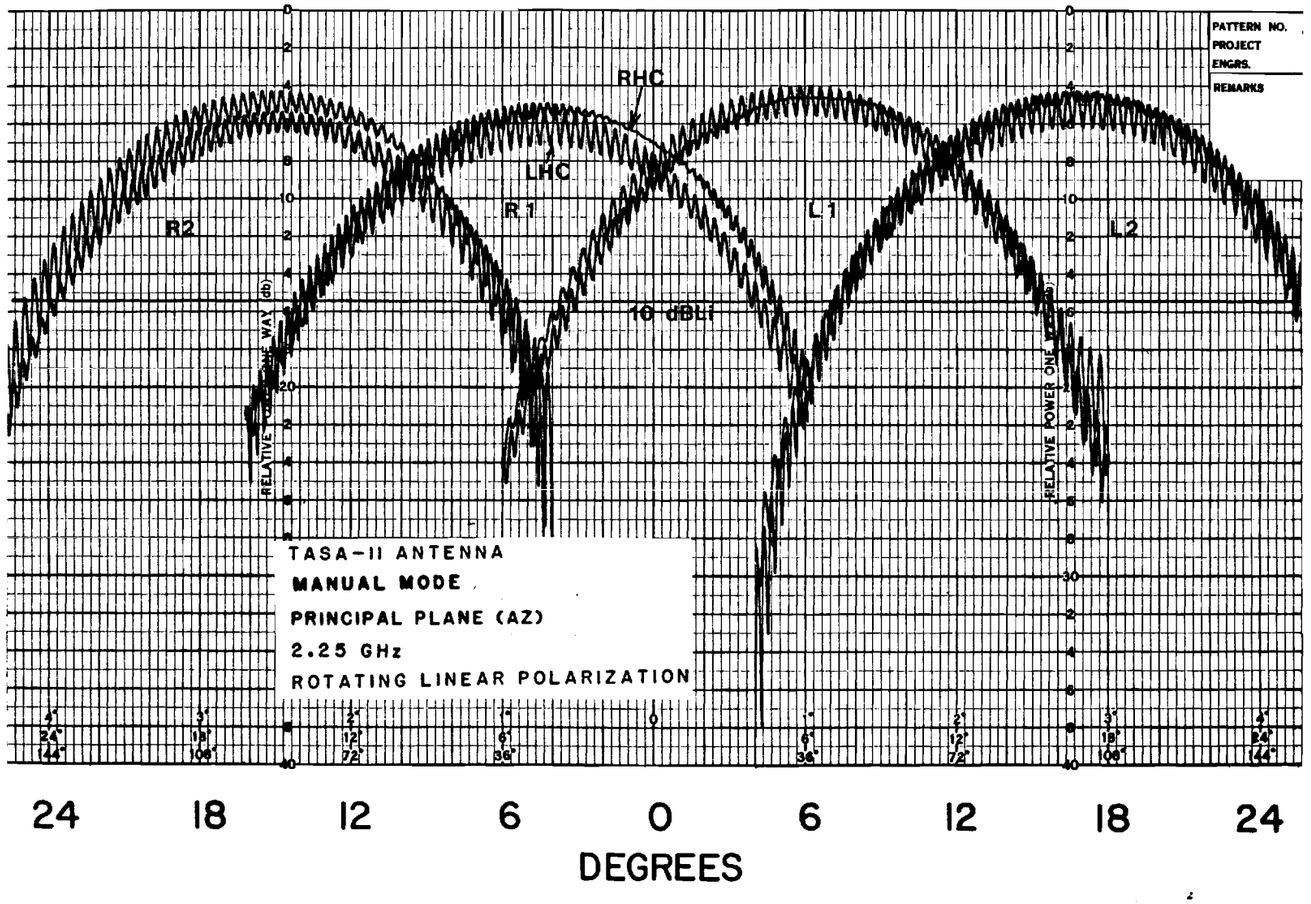

Figure 25. Principal plane (AZ) pattern (RLP) at 2.25 GHz in the manual mode.

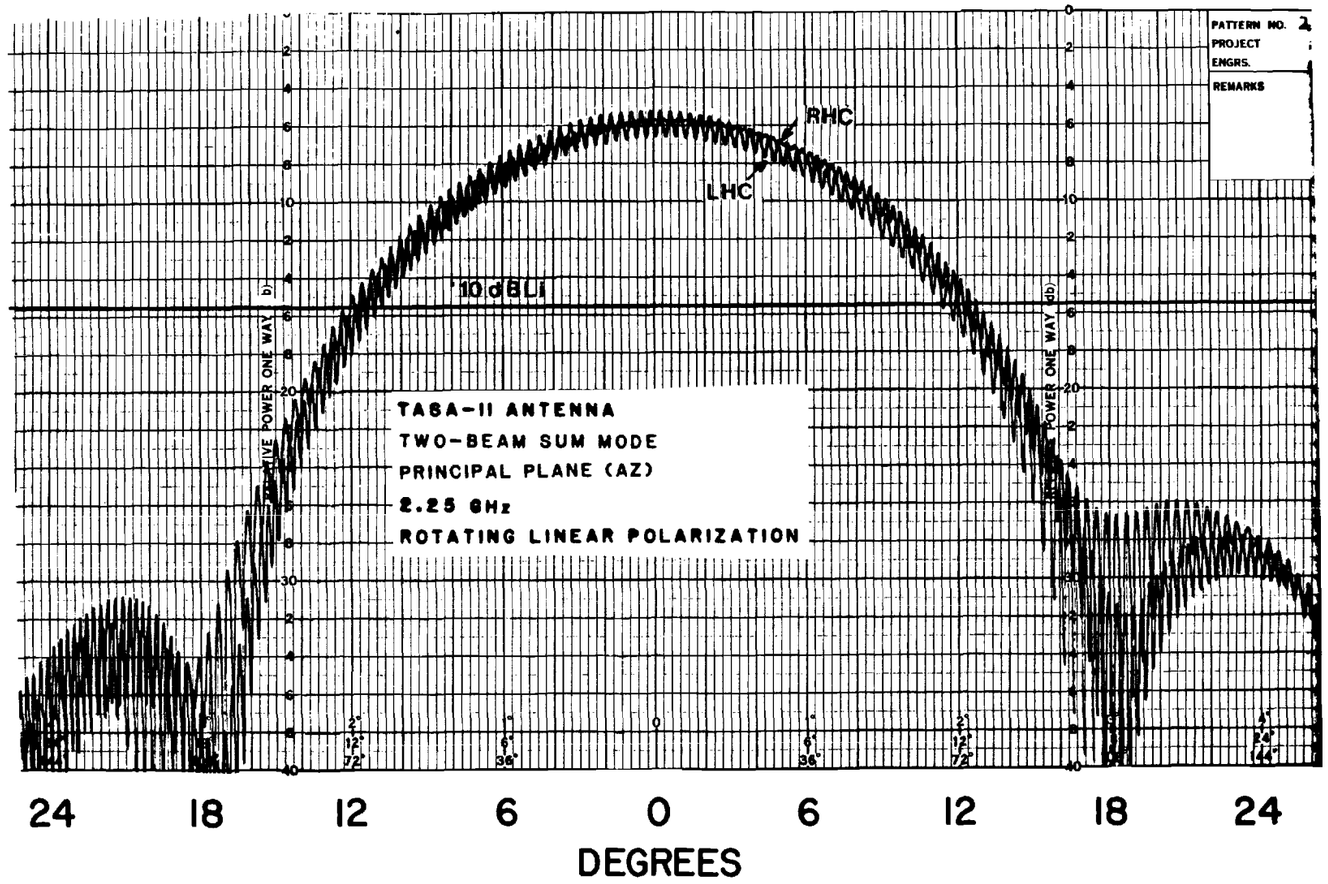

Figure 26. Principal plane (AZ) pattern (RLP) at 2.25 GHz in the two-beam sum mode.

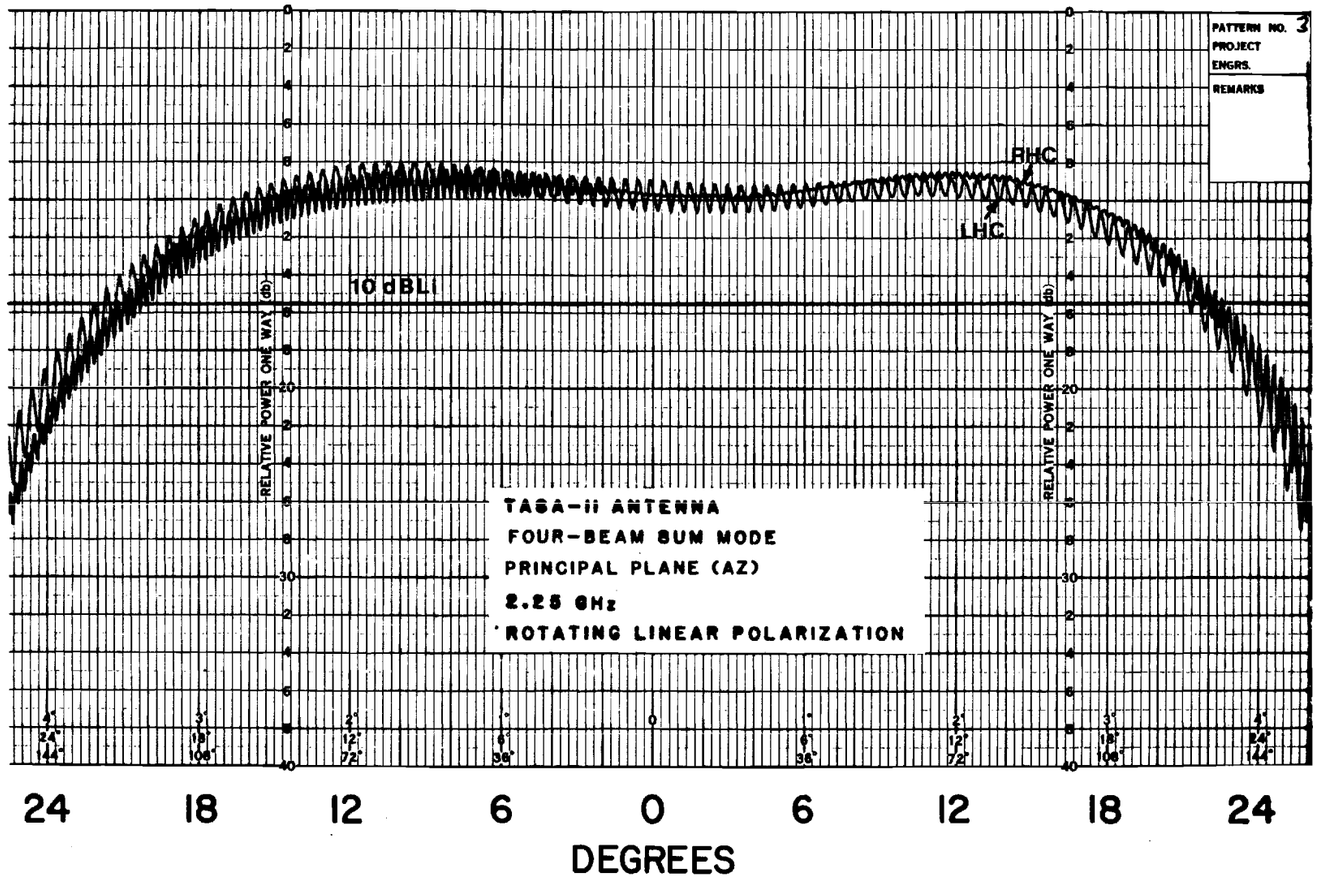

Figure 27. Principal plane (AZ) pattern (RLP) at 2.25 GHz in the four-beam sum mode.

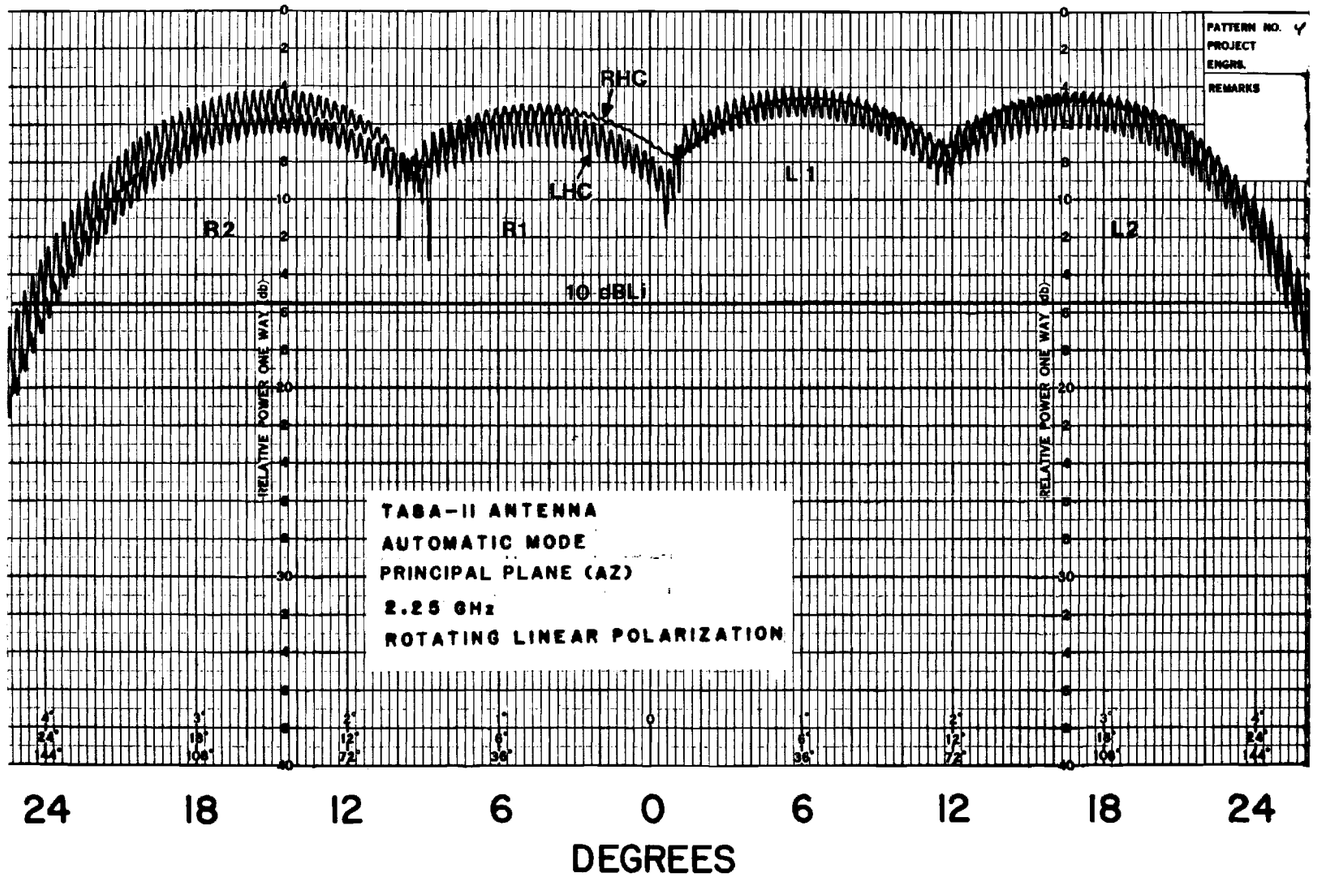

Figure 28. Principal plane (AZ) pattern (RLP) at 2.25 GHz in the automatic mode.

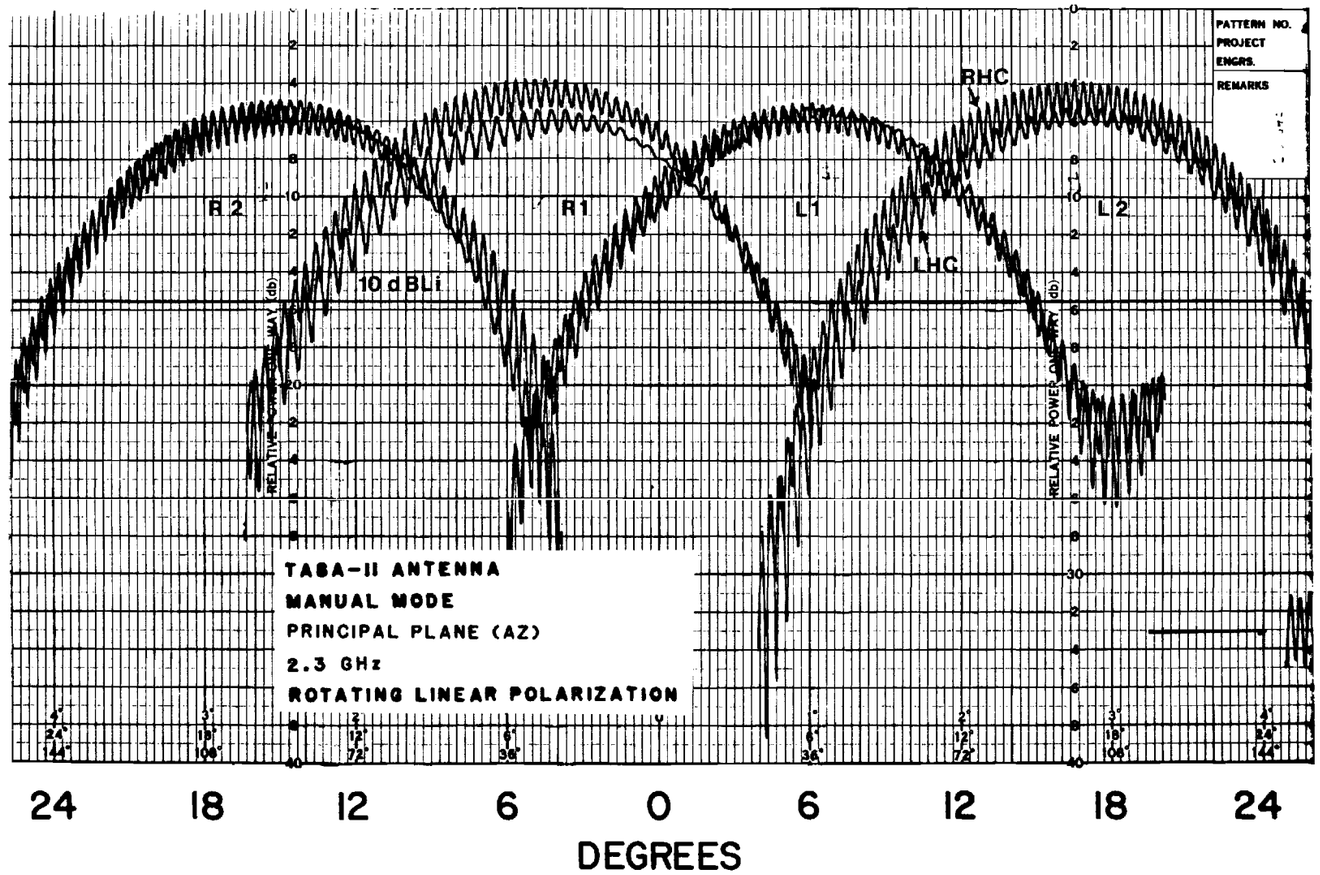

Figure 29. Principal plane (AZ) pattern (RLP) at 2.3 GHz in the manual mode.

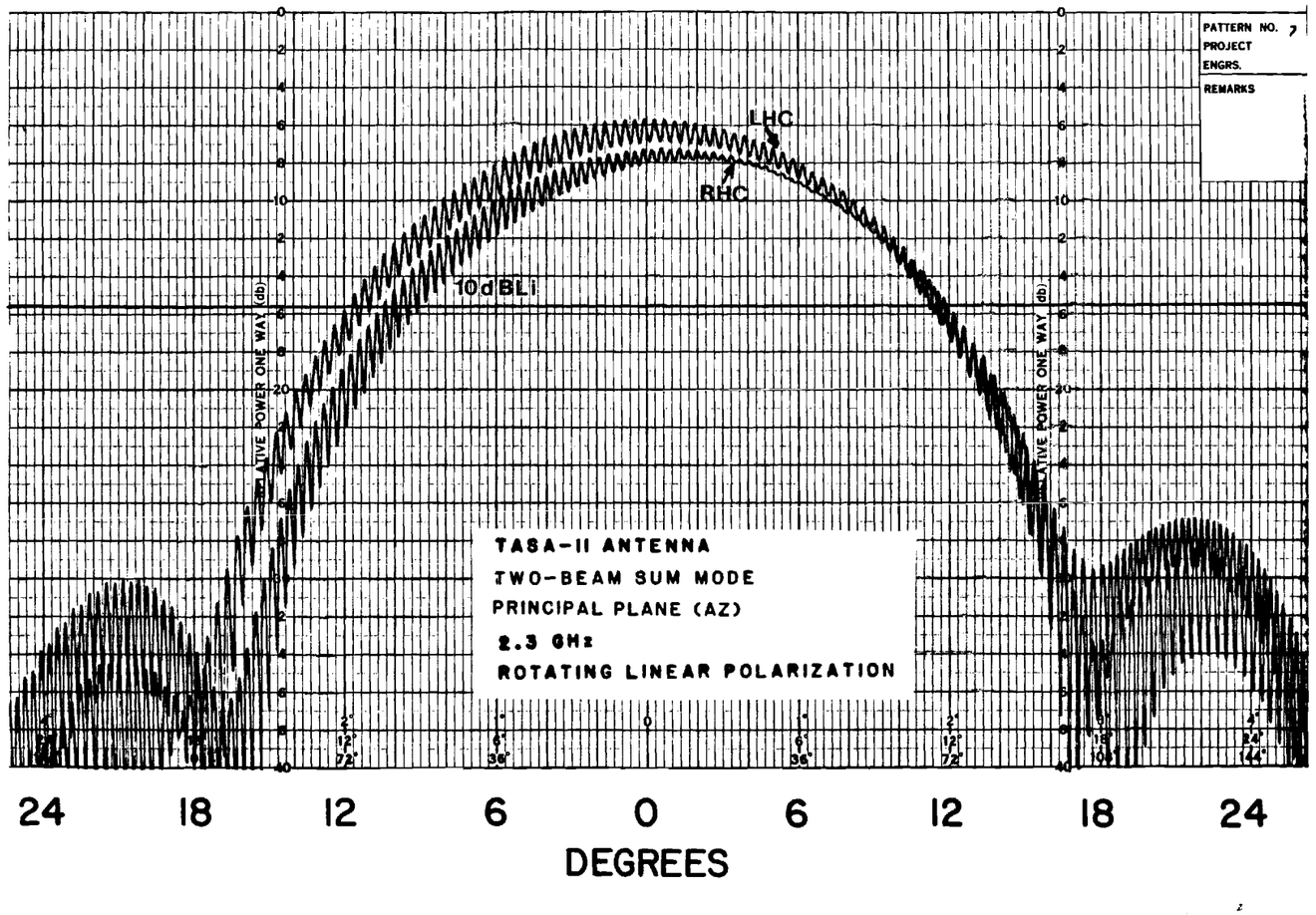

Figure 30. Principal plane (AZ) pattern (RLP) at 2.3 GHz in the two-beam sum mode.

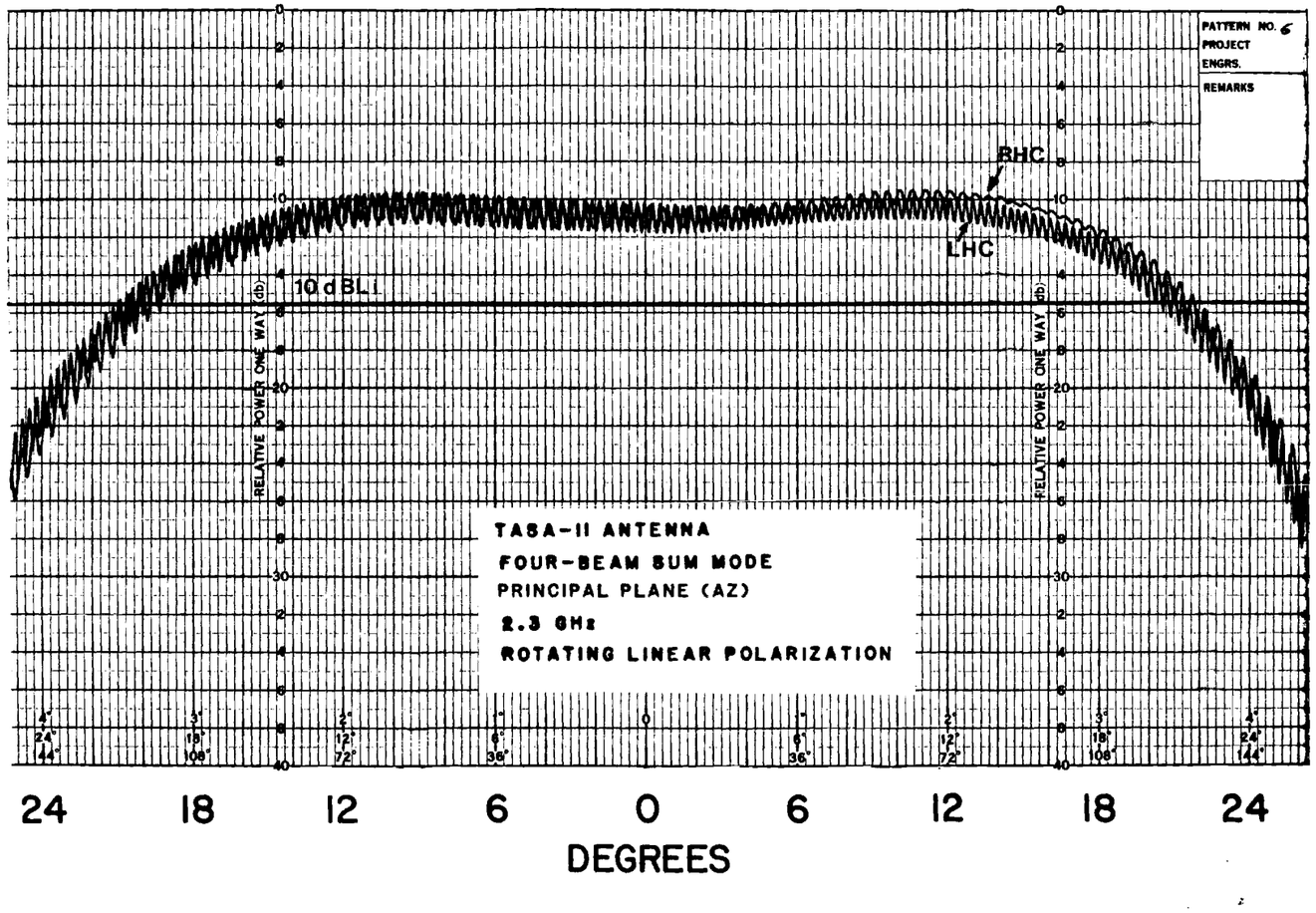

Figure 31. Principal plane (AZ) pattern (RLP) at 2.3 GHz in the four-beam sum mode.

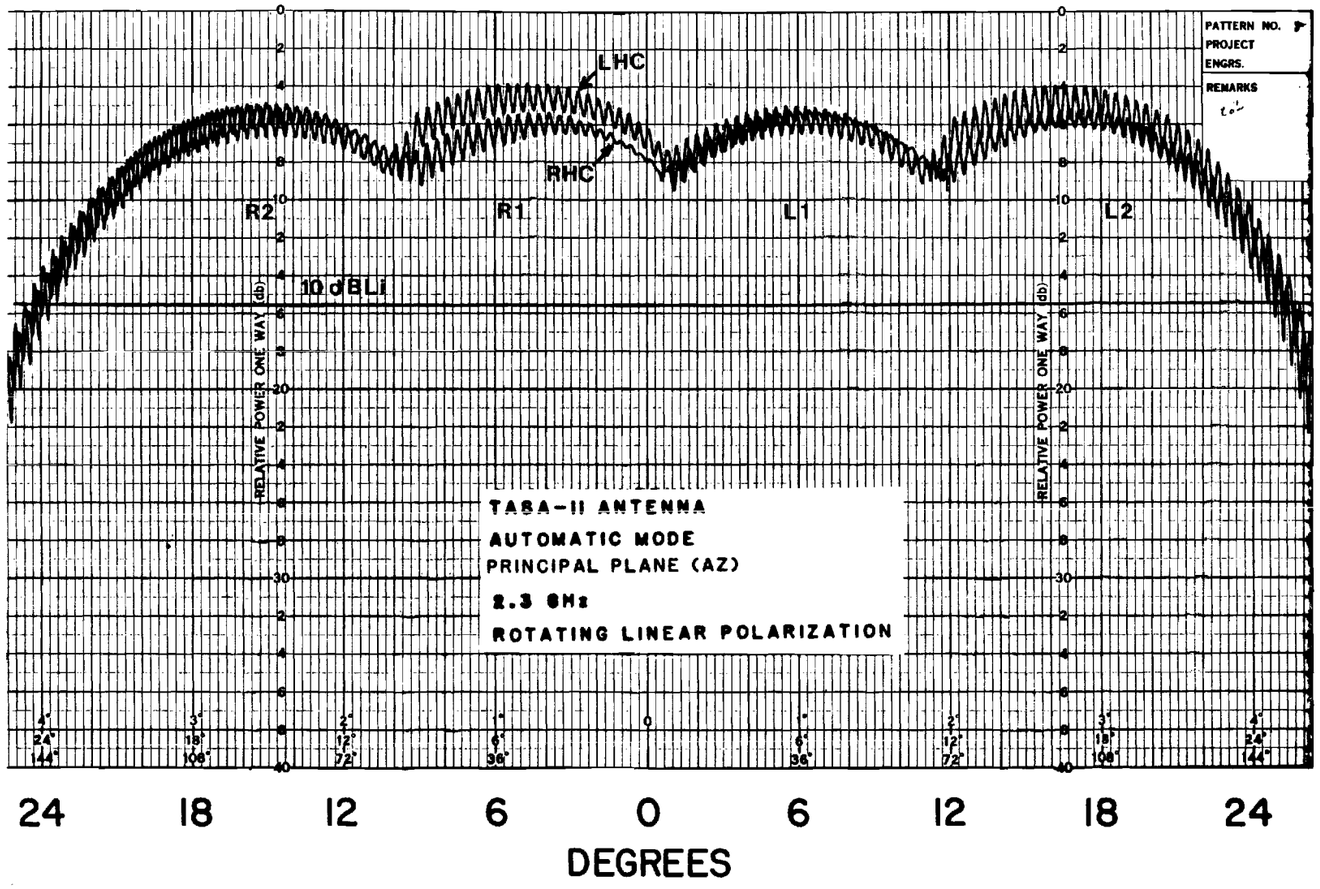

Figure 32. Principal plane (AZ) pattern (RLP) at 2.3 GHz in the automatic mode.

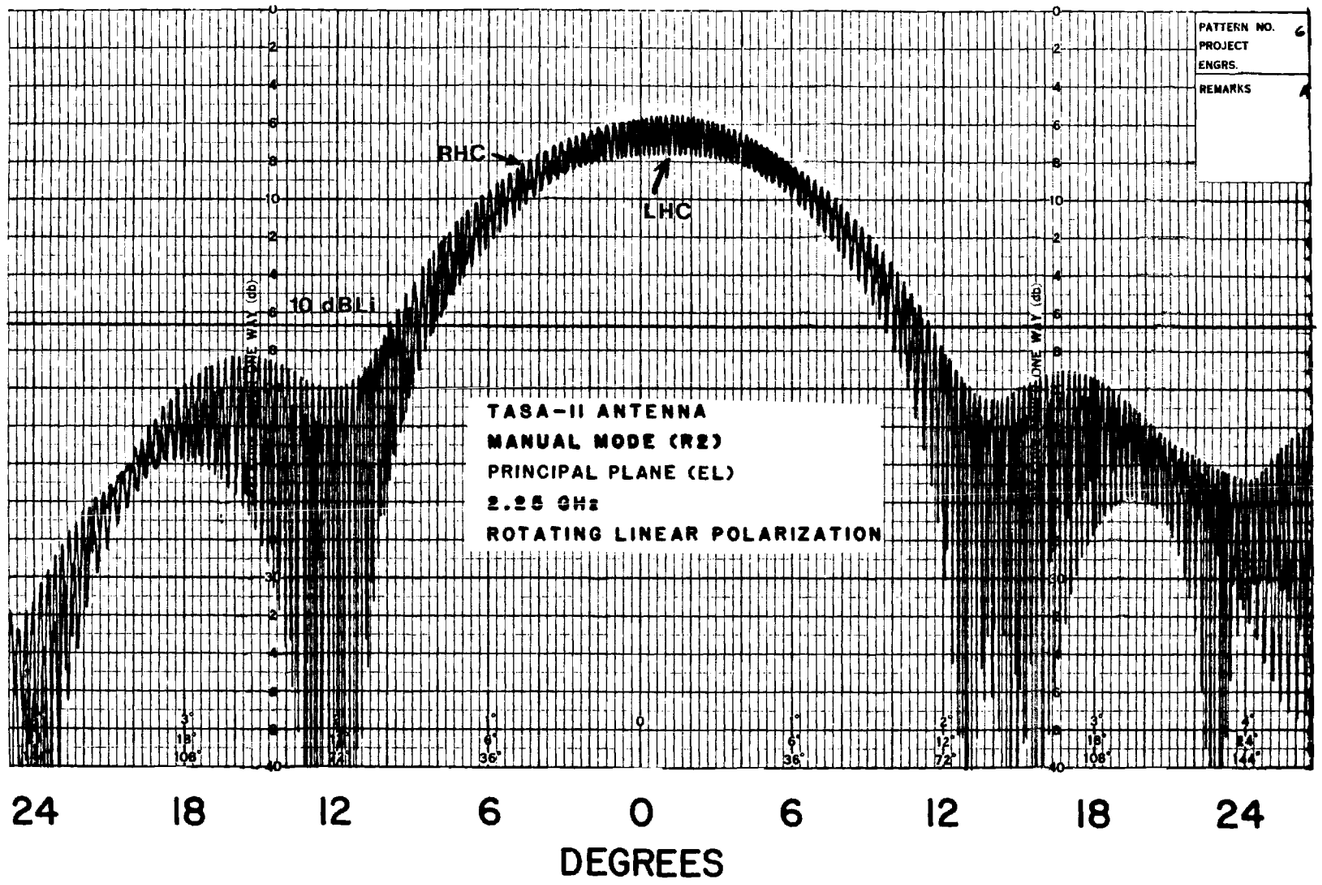

Figure 33. Principal plane (EL) pattern (RLP) at 2.25 GHz in the manual mode (beam R2).

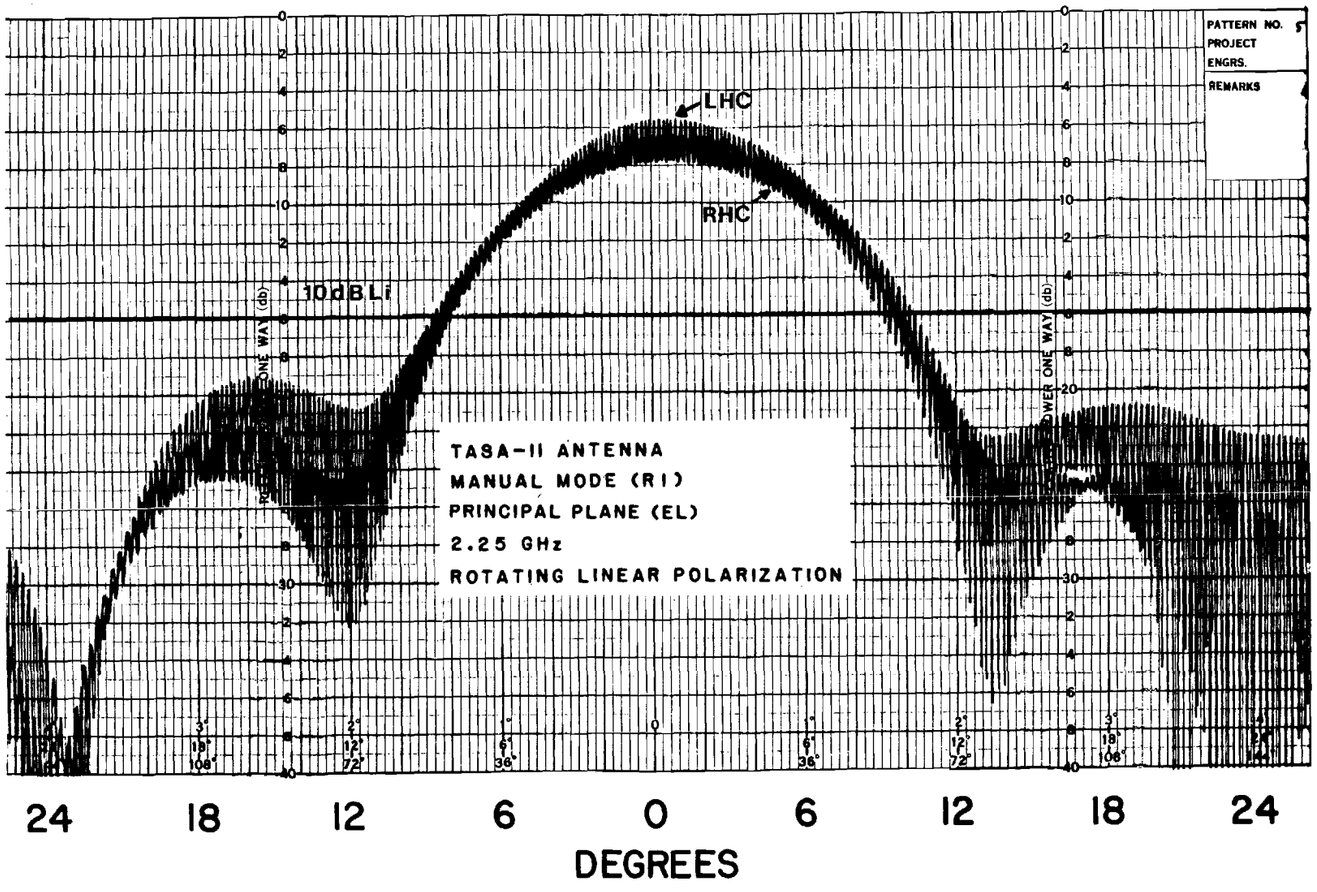

Figure 34. Principal plane (EL) pattern (RLP) at 2.25 GHz in the manual mode (beam R1).

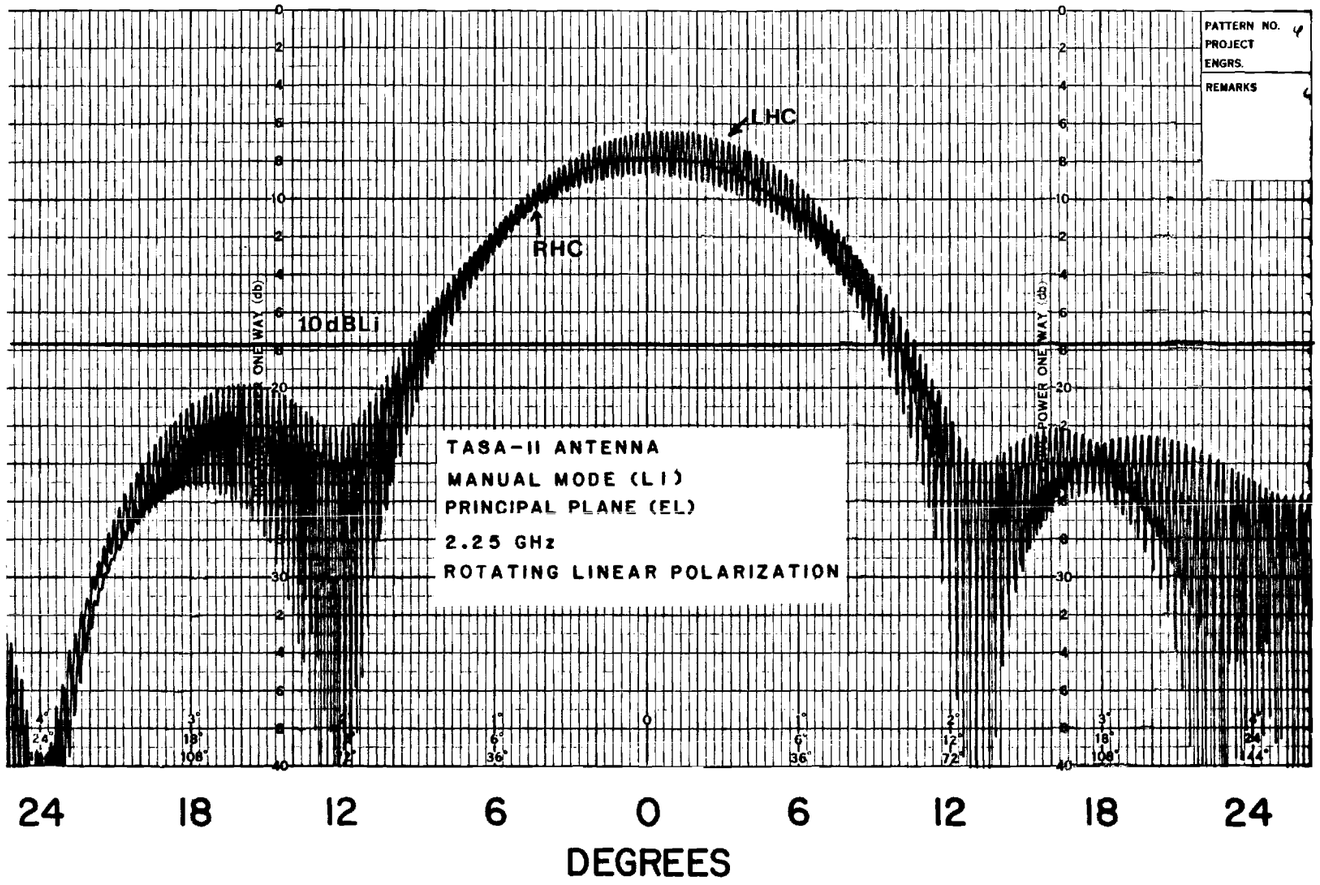

Figure 35. Principal plane (EL) pattern (RLP) at 2.25 GHz in the manual mode (beam L1).

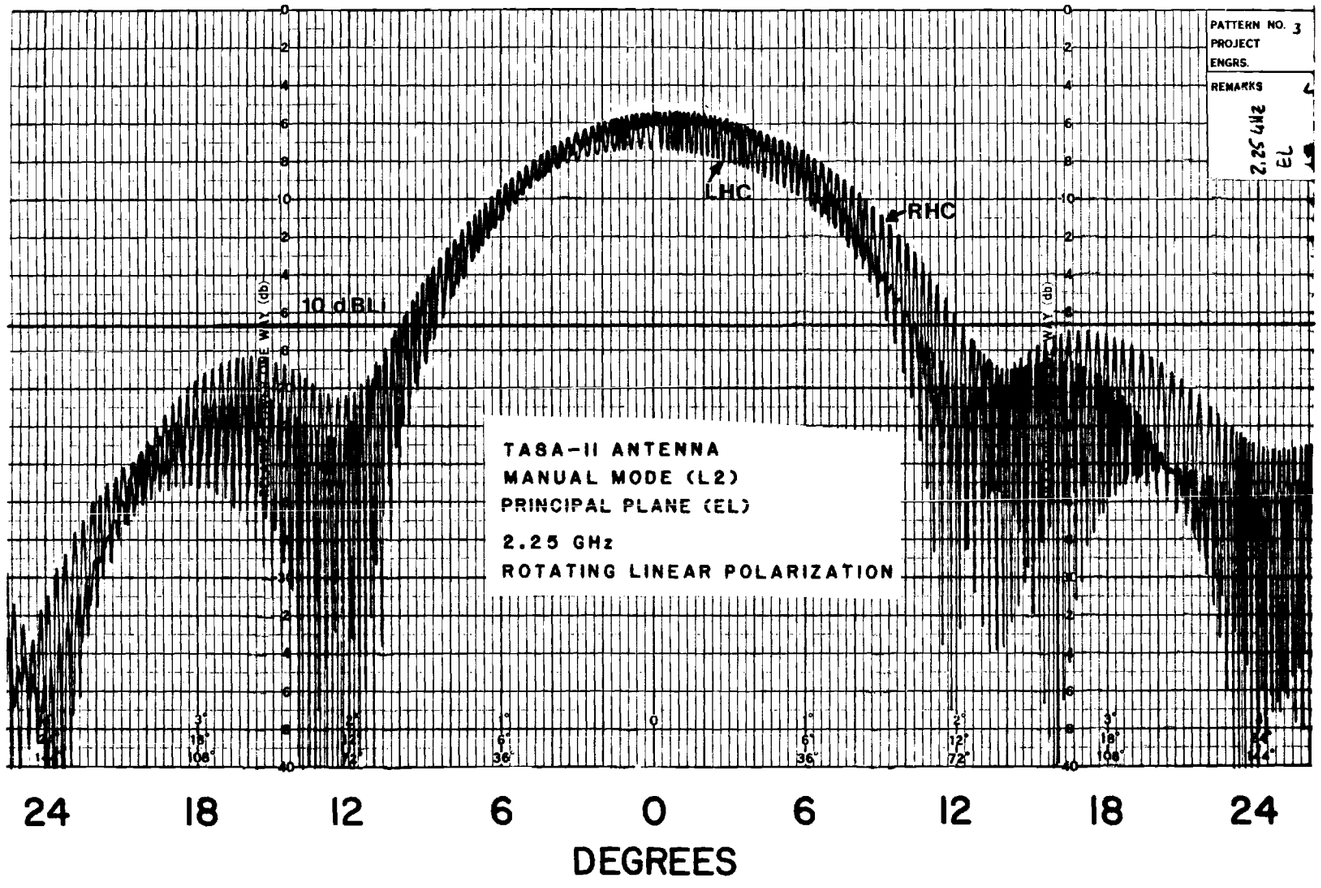

Figure 36. Principal plane (EL) pattern (RLP) at 2.25 GHz in the manual mode (beam L2).

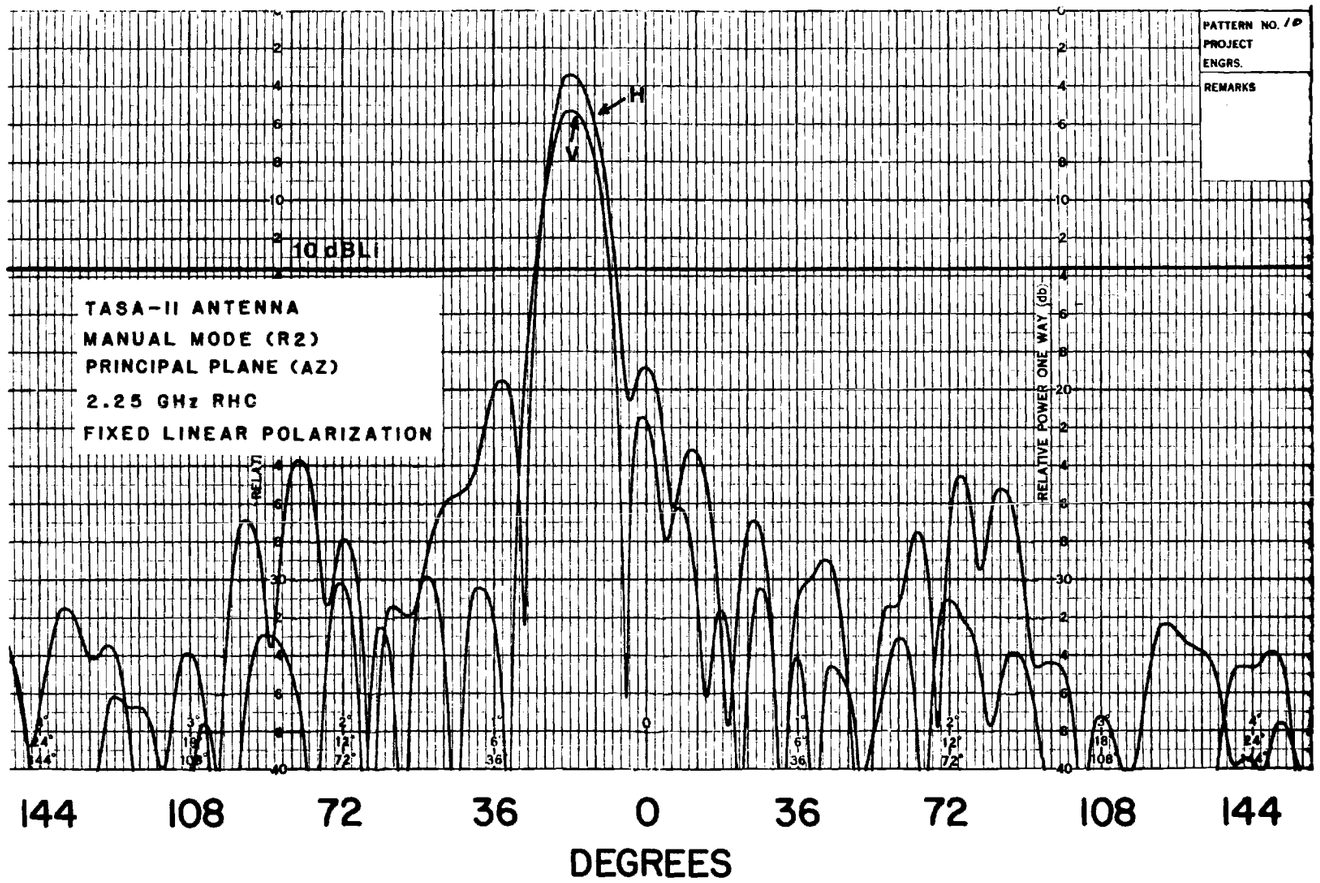

Figure 37. Principal plane (AZ) pattern (FLP) at 2.25 GHz (RHC) in the manual mode (beam R2).

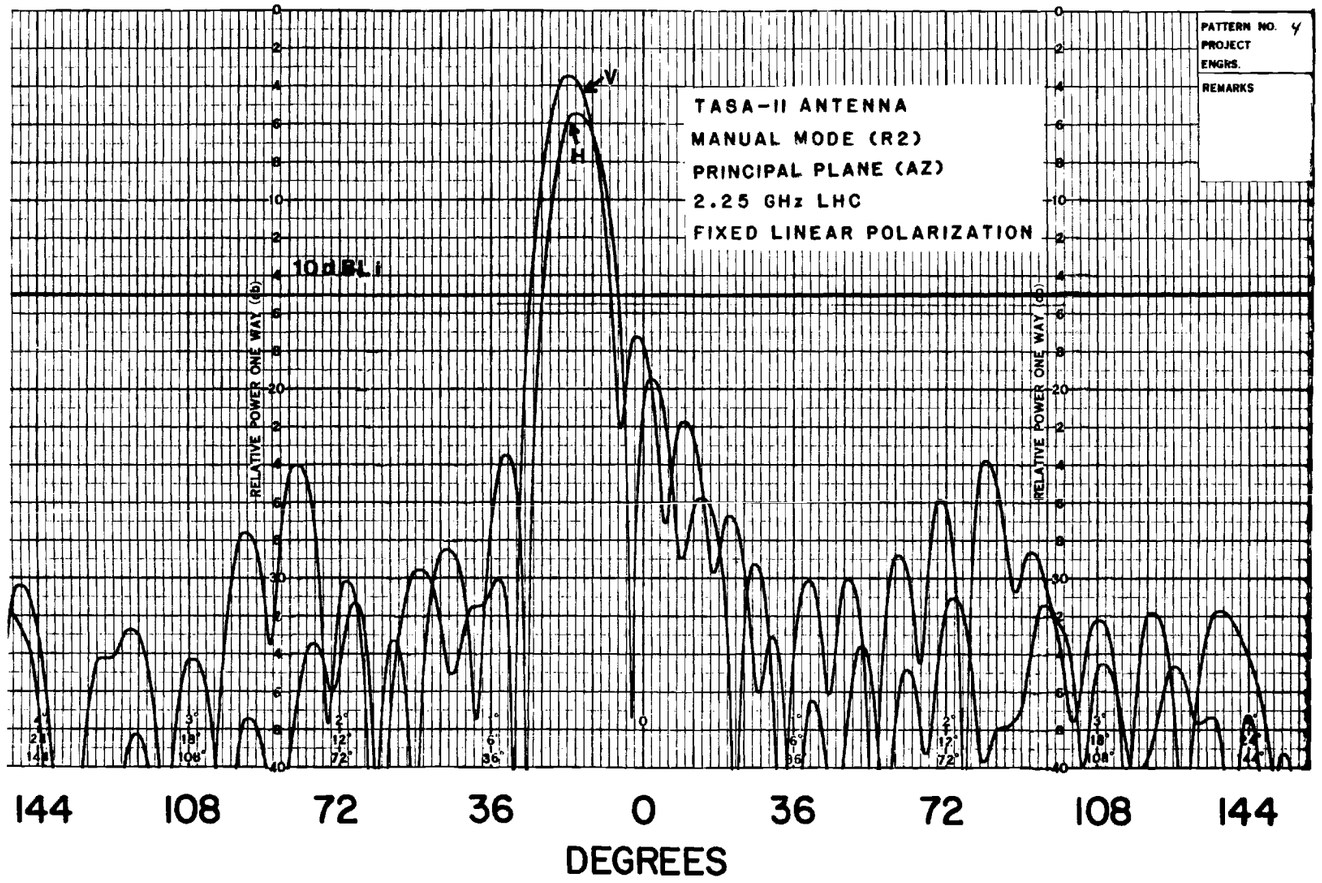

Figure 38. Principal plane (AZ) pattern (FLP) at 2.25 GHz (LHC) in the manual mode (beam R2).

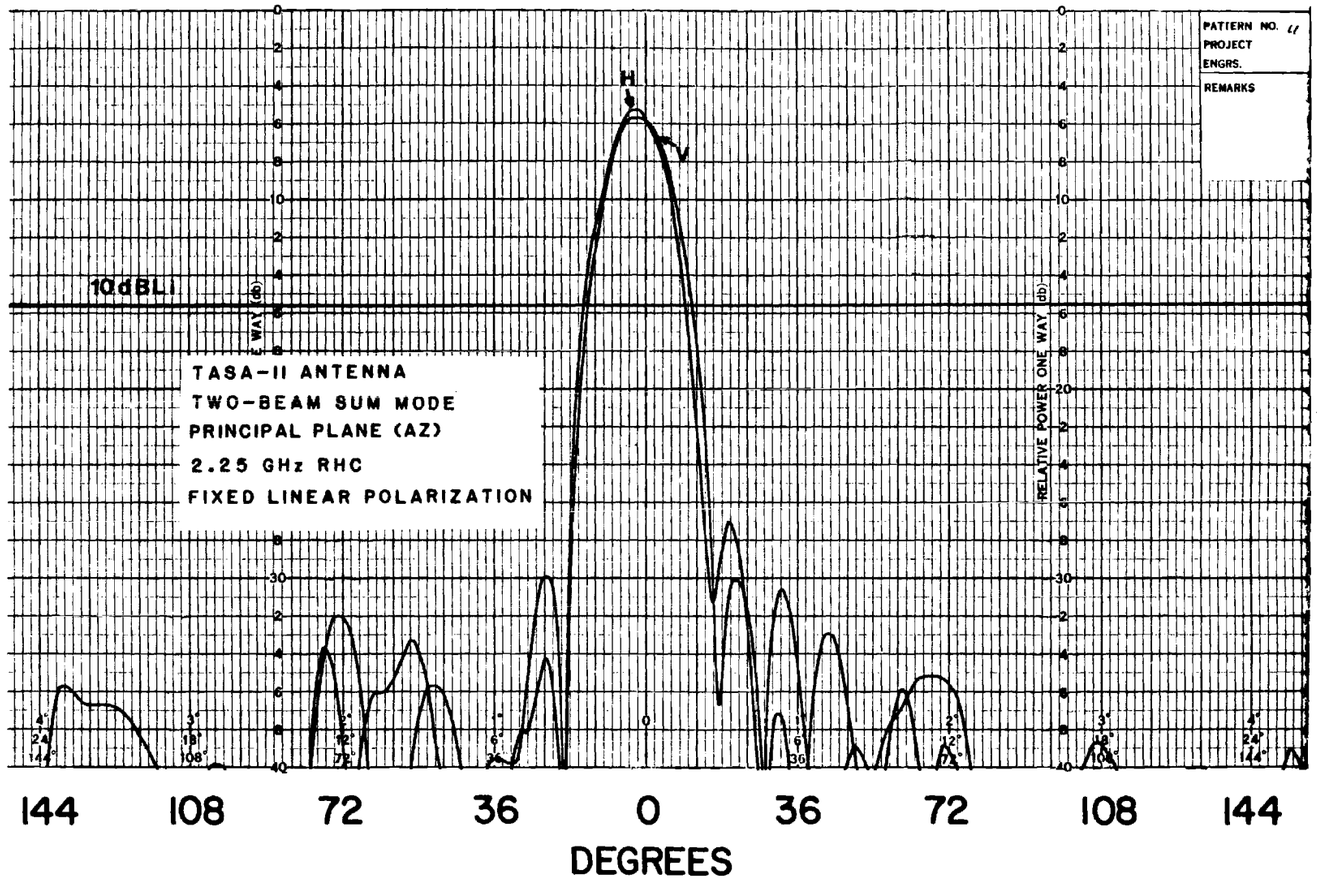

Figure 39. Principal plane (AZ) pattern (FLP) at 2.25 GHz (RHC) in the two-beam sum mode.

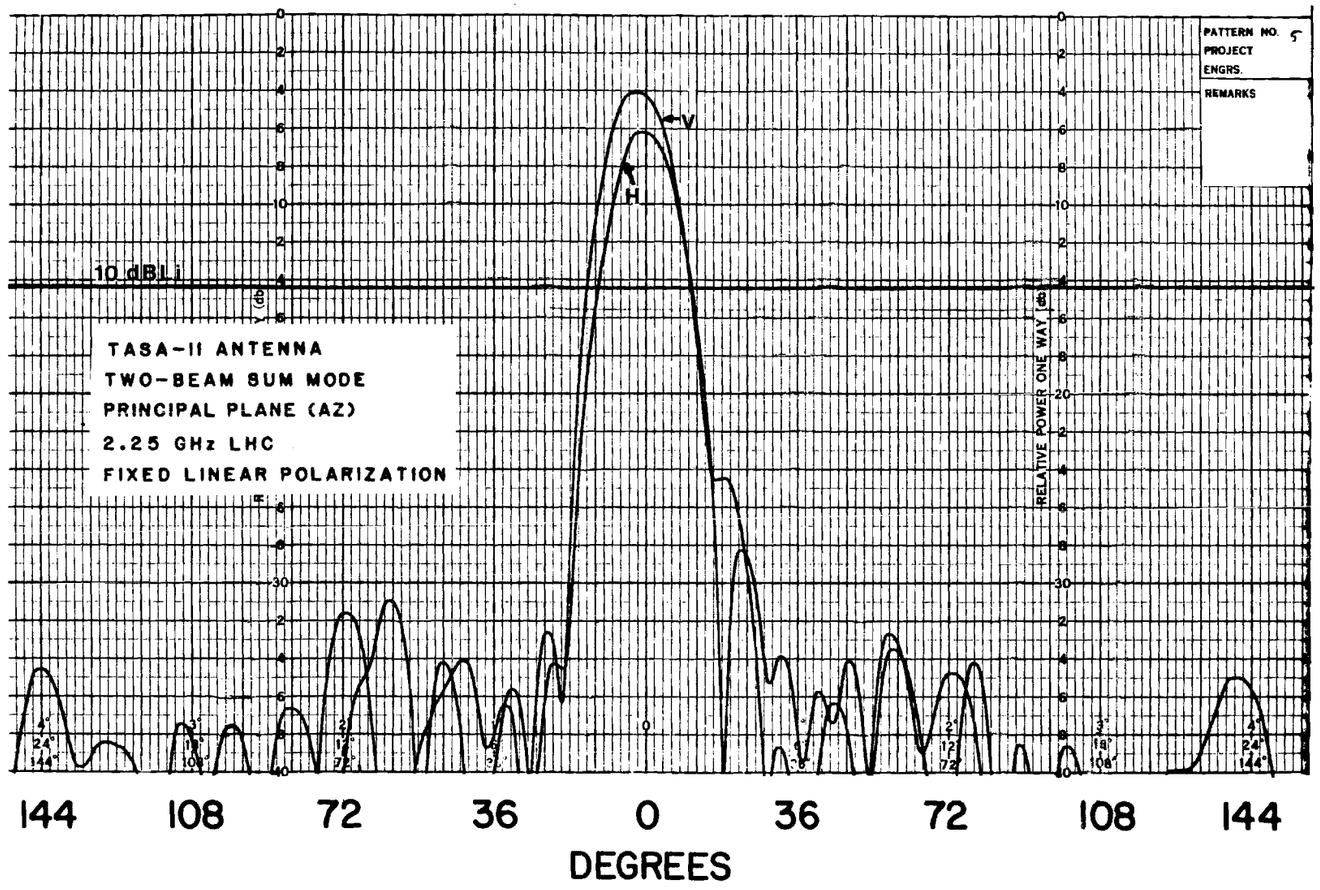

Figure 40. Principal plane (AZ) pattern (FLP) at 2.25 GHz (LHC) in the two-beam sum mode.

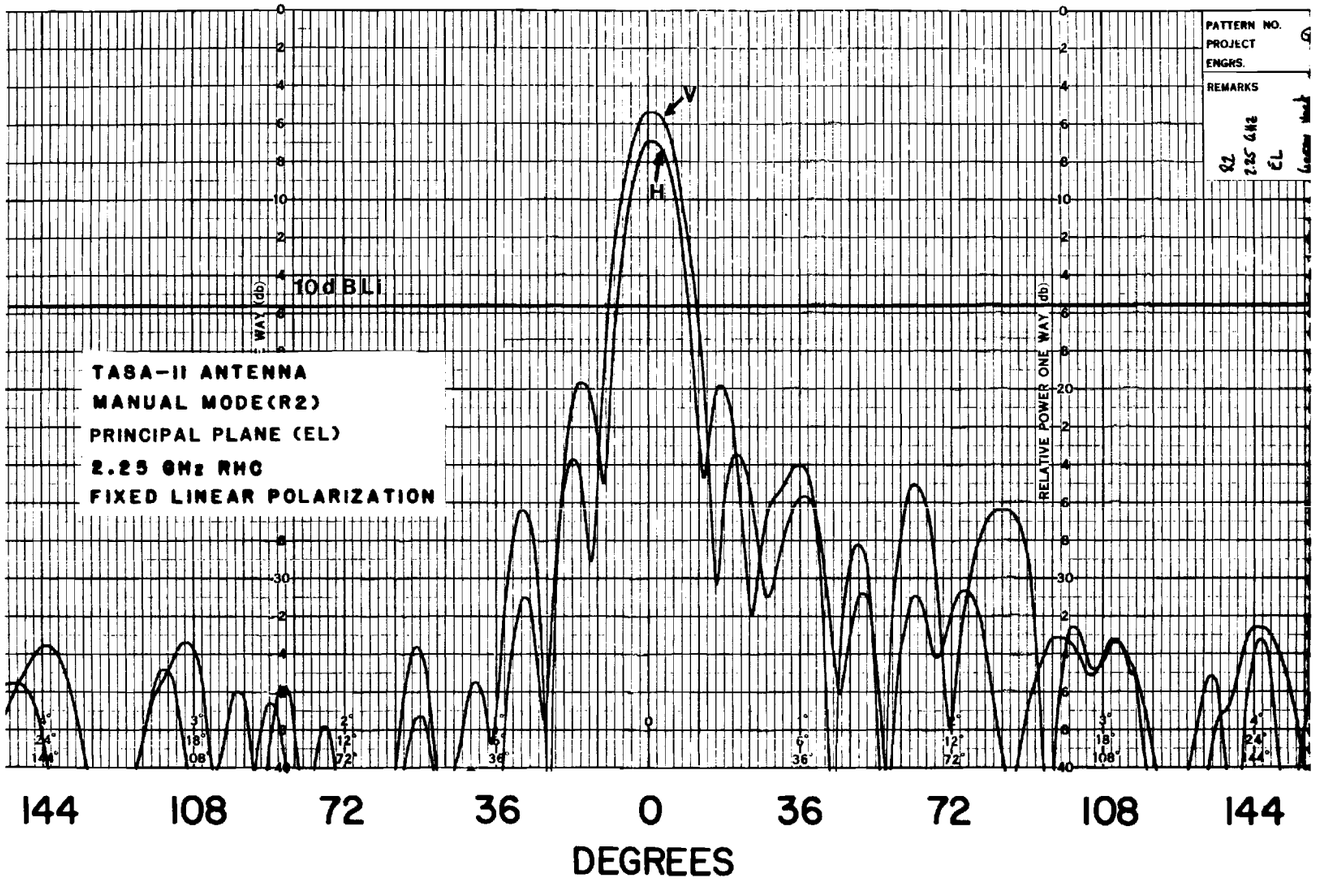

Figure 41. Principal plane (EL) pattern (FLP) at 2.25 GHz (RHC) in the manual mode (beam R2).

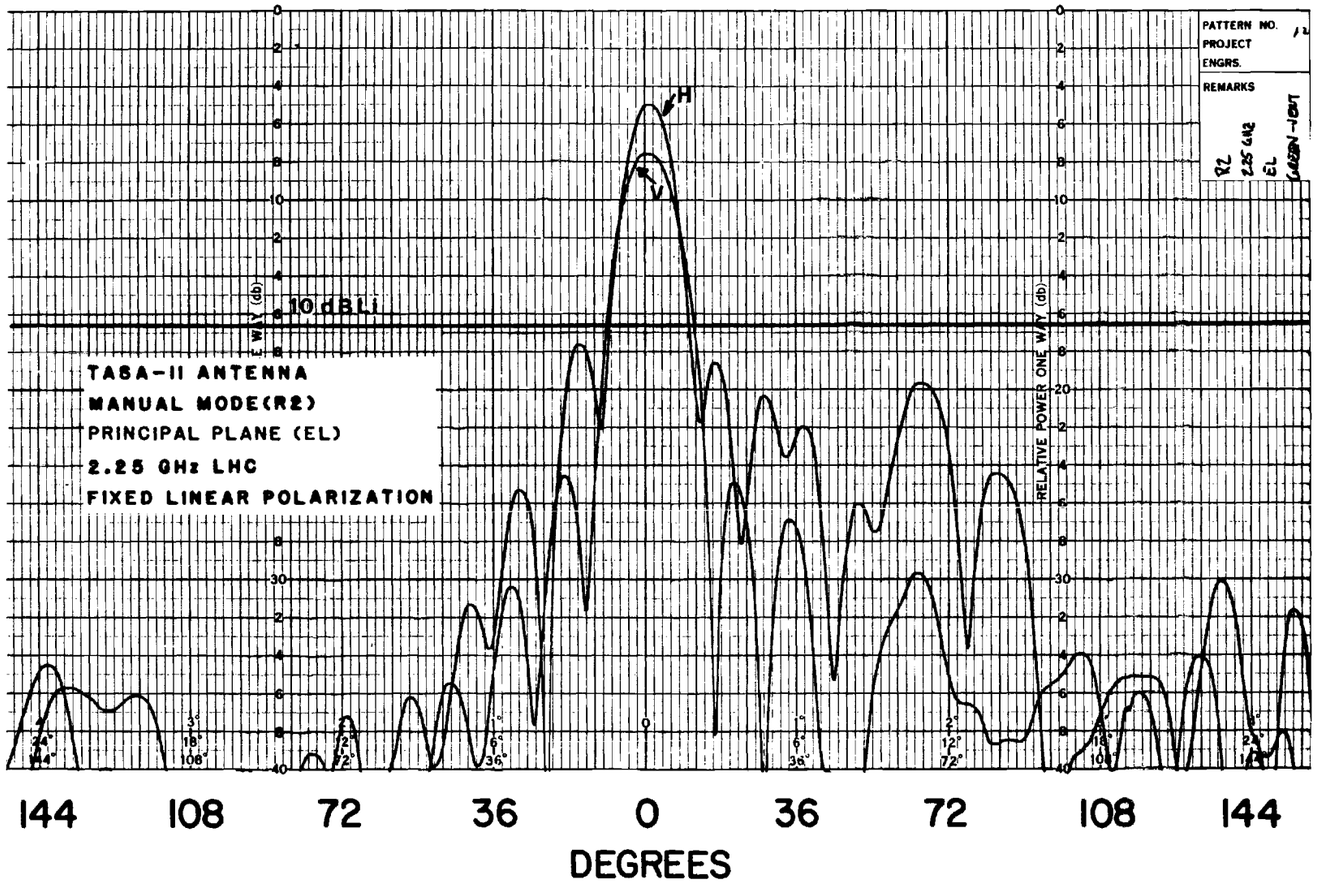

Figure 42. Principal plane (EL) pattern (FLP) at 2.25 GHz (LHC) in the manual mode (beam R2).

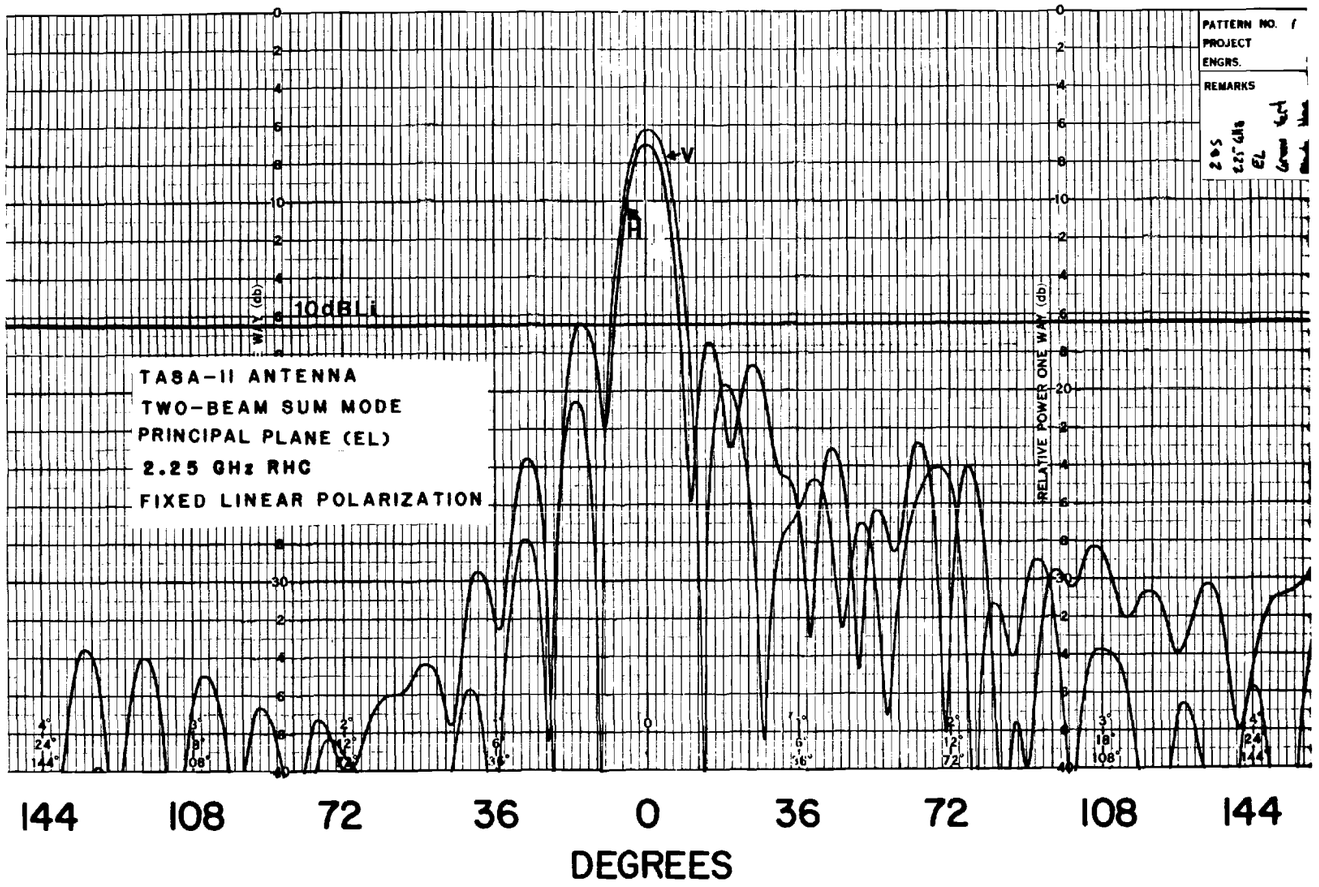

Figure 43. Principal plane (EL) pattern (FLP) at 2.25 GHz (RHC) in the two-beam sum mode.

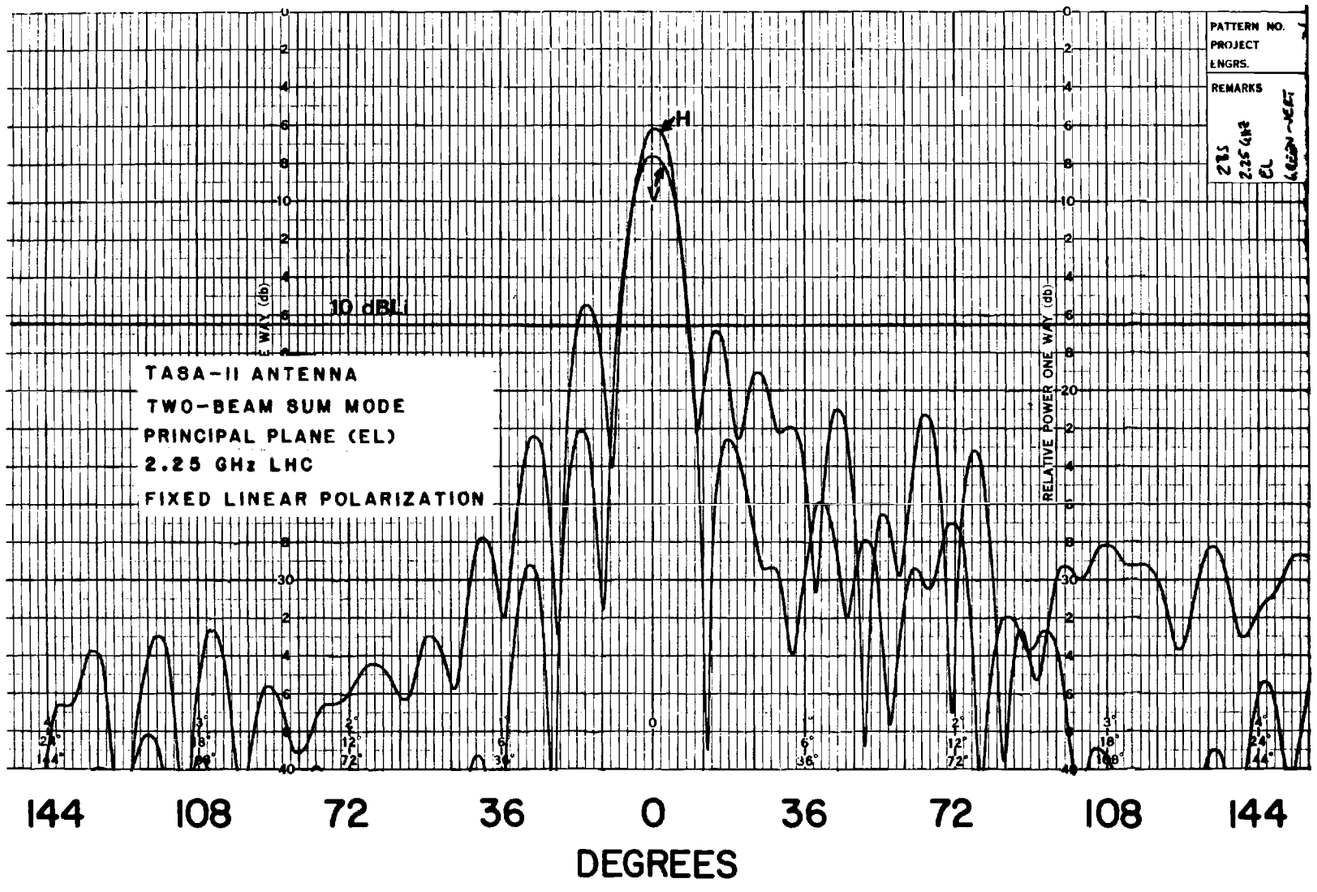

Figure 44. Principal plane (EL) pattern (FLP) at 2.25 GHz (LHC) in the two-beam sum mode.